공학석사학위논문

Room Temperature Hydrogen Storage in a Metal-Organic Framework-derived Carbon-based Hybrid material

2015 년 2 월

서울대학교 대학원

재료공학부

Gueye, Magatte Niang

Room Temperature Hydrogen Storage in a Metal-Organic Framework-Derived Carbon-Based Hybrid Material

지도 교수 박 종 래

이 논문을 공학석사 학위논문으로 제출함
2014년 10월

서울대학교 대학원
재료공학부
Gueye Magatte Niang

Gueye Magatte Niang의 석사 학위논문을
인준함
2014년 12월

위 원 장 _____ 장 지 영 _____ (인)

부위원장 _____ 박 종 래 _____ (인)

위 원 _____ 남 기 태 _____ (인)

Abstract

Room temperature Hydrogen Storage in a Metal-Organic Framework-Based Hybrid Material

Gueye, Magatte Niang
Department of Material Science and Engineering
The Graduate School
Seoul National University

In addressing the global demand for clean and renewable energy, hydrogen stands as a promising candidate for many fuel cell applications. In order to use it at an industrial scale, researchers must develop practical and efficient storage systems that fulfill the targets stated by the US Department of Energy.

Among the storage systems that have emerged in the past decades, porous materials have attracted researchers' interest due to their light weight, fast sorption kinetics, total reversibility and mass production capacity. They however store only a small amount of hydrogen at room temperature. In order to overcome that drawback related to the storage capacity, researchers have been synthesizing hybrid materials as they could show enhanced characteristics which would lead to an enhanced storage.

Hybridizing can be achieved by including metal nanoparticles into the porous materials so that spillover can occur: dissociation of the hydrogen molecule on the metal followed by migration and further diffusion on the porous material. This phenomenon, well established in the catalyst field, remains however highly controversial in hydrogen storage as some authors reported huge enhancement while others noticed bare or no enhancement at all. Such discrepancies in the literature suggest a high dependency of spillover occurrence with the hybrid material characteristics and hence will persist until the true conditions, which favor enhancement, as well as the mechanism, get revealed. Numerous reports about different materials under different conditions could then lead to a better understanding of that phenomenon.

Many porous materials have been studied to show an enhancement resulting from the metal doping. When seeking for an enhancement, it might be more interesting to choose the material which stores an appreciable amount of hydrogen, if not the highest, but quite surprisingly, no research has been done on MDCs, highly porous carbon materials with exceptional hierarchical porosity and high SSA, which store the highest amount of hydrogen in their structure at room temperature and 100 bar.

Moreover, the electronic state of the doping metal has not been studied either in spite of the relative importance of the metal form or the oxide form in hydrogenation processes. Previous works did not outline which state of the metal was expected to play a role in the enhancement process, or actually did.

This work then aims to give the first evidence of the feasibility of MDC hybridization by platinum particles, which will be wanted to be in a metal form. A special care will be given to the synthesis method as MDC's synthesis requires harsh thermal treatment that might be disadvantageous to the Pt particles.

The obtained results showing an increased storage capacity of the hybrid material compared to the pristine one, together with fast kinetics and total reversibility, will be presented in this work. Before that, the different hydrogen storage systems will be briefly reviewed in a first step, the state of the arts of storage enhancement by metal doping will be presented in a second step and a deeper explanation of the purpose of this work as well as the experimental methods explanation will be given afterwards.

Keywords: hydrogen storage, spillover, metal-organic frameworks-derived carbons, hybrid materials.
Student Number: 2013-23811

Contents

List of abbreviations

AC: Activated carbon

BDC: Terephtalic acid

BET: Brunauer-Emmett-Teller

CGH_2: Compressed gaseous hydrogen

CNT: Carbon nanotubes

GO: graphene oxide

LH_2: Liquid hydrogen

MDC: Metal-organic framework-derived carbon

MOF: Metal-organic framework

MWCNT / MWNT: multiwalled carbon nanotubes

Pt@rGO: Platinum-doped reduced graphene oxide

Pt-MDC: Platinum particles incorporated into MDC's framework

Pt-MOF: Platinum particles incorporated into MOF's framework

Pt@rGO-MDC: Platinum-doped reduced graphene oxide flakes incorporated into MDC

Pt@rGO-MOF: Platinum-doped reduced graphene oxide flakes incorporated into MOF

PXRD: Powder X-Ray diffraction

rGO: Reduced graphene oxide

rGO-MDC: reduced graphene oxide flakes incorporated into MDC

rGO-MOF: reduced graphene oxide flakes incorporated into MOF

SBU: Single building unit

SEM: Scanning Electron Microscopy

SSA: specific surface area

SWCNT /SWNT: single walled carbon nanotubes

TEM: Transition Electron Microscopy

U.S. DOE: United States Department of Energy

XPS: X-Ray photospectrometry

ZTC: Zeolite-template carbon

List of tables

List of figures

1. Introduction

1.1. Hydrogen economy

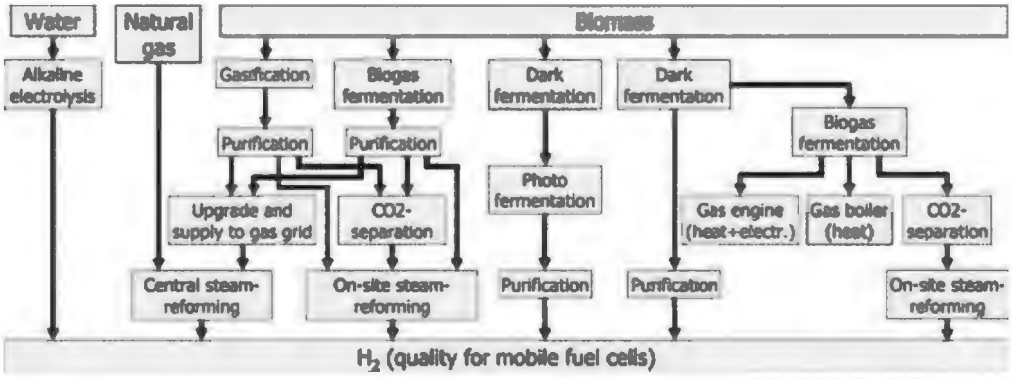

Figure 1:Hydrogen production [1]

As the global energy demand is increasing while the fossil fuels are rapidly depleting, their prices rising accordingly and their use causing environmental issues, a cheap, sustainable and eco-friendly alternative is needed. Hydrogen could be that alternative. Indeed it is the most abundant chemical element in the universe ,its combustion with oxygen ($2H_2^g + O_2^g \rightarrow 2H_2O$) produces only water and energy (120 kJ/g) without releasing any harmful by-products, and it has the highest energy density per mass among all hydrogen-based fuels (three times that of gasoline, see **Table 1**). Transitioning to a hydrogen economy, an economy system where hydrogen is used as fuel, seems then a

promising way to answer the challenges which arise from the global energy demand.

Table 1: Energy contents of different fuels [2]

Fuel	Energy content (MJ/kg)
Hydrogen	120
Liquefied natural gas	54.4
Propane	49.6
Aviation gasoline	46.8
Automotive gasoline	46.4
Automotive diesel	45.6
Ethanol	29.6
Methanol	19.7
Coke	27
Wood (dry)	16.2
Bagasse	9.6

Such a transition faces yet a number of barriers. As hydrogen does not occur naturally, it is only an energy carrier and needs to be produced. The main part of the current hydrogen production (Figure 1) is through natural gas reforming, which does not prevent from carbon emissions but only transfers them from the user (vehicle) to the plant. Clean

productions means, such as water splitting by solar energy, do exist but are only lab scale applications and effort must further be done in a carbon neutral hydrogen production.

The main reason that prevents a transition to a hydrogen economy remains however its storage. Despite its high energy density per mass, hydrogen has a low density (0.08988 kg/m^3), and while 1 kg of hydrogen could replace 3 kg of gasoline, 3500 gallons are needed for one gallon gasoline (3.79 L) [3]. Storing hydrogen as is would require huge tanks which are not practical for on board applications. Efficient storage systems have then to be implemented for hydrogen to be used as a fuel for on-board applications.

The US Department of energy stated the storage requirements that define such an efficient storage system. They are set under the assumptions that future light-duty vehicles should at least be as much performant as today ones and hence should stand driving range greater than 500km at once and should operate under ambient conditions while being compact, safe, cheap, performant and competitive. The 2017 targets, summarized in **Table 2**, were set taking into account the recent technologies and advances in the hydrogen storage research community. As it can be seen in that table, an efficient storage system should store at least 5.5 wt.% H_2 at ambient conditions.

Table 2: Summary of US DOE technical system targets for on-board hydrogen storage for, adapted from [4]

Storage parameter	Unit	2017	Ultimate
System gravimetric capacity	wt. %	5.5 (1.8 kWh/kg)	7.5 (2.5 kWh/kg)
System volumetric capacity	g/l	40 (1.3 kWh/L)	70 (2.3 kWh/L)
Fuel cost	$/gge at pump	2~4 ($2/kWh)	2~4 ($2/kWh)
Min/ Max delivery temperature	°C	-40/85	-40/85
Operational cycle life (1/4 tank to full)	Cycles	1500	1500
Min/ Max delivery pressure from storage system	Bars	5/12	3/12
System fill time (5 kg)	Min	3.3	2.5

Three main storage systems have emerged in the past years: compressed gaseous hydrogen, liquid hydrogen and solid state hydrogen which comprises hydrides and porous materials.

1.2. Overview of current hydrogen storage systems

1.2.1. Compressed gaseous hydrogen (CGH_2)

For a light duty vehicle to drive over 500 km without further charging, around 5 kg H_2 is needed. Given its low density, such a high amount can be stored at room temperature only if the pressure is increased. Compressed gaseous hydrogen (CGH_2) designates such a storage system where highly pressurized hydrogen gas is contained in a vessel at pressure from 350 up to 700 bar. This upper limit is mainly due to the validity of the perfect gas equation rather than technological issues. As it can be seen in Figure 2, from 700 bar, the real gas behavior deviates so much from the perfect gas one that the increased demands on the pressure container are not justified by the small energy increase (Figure 3).

With such high operating pressures, special vessels need to be developed. Ideally these tanks should be spherical for energy minimization. However regarding the available space in a car, a cylinder is more suitable. For such geometry, longitudinal stresses are the most important parameters governing the tank walls' thickness and hence in order to increase the amount stored, it is preferable to increase the vessel's length rather than its diameter.

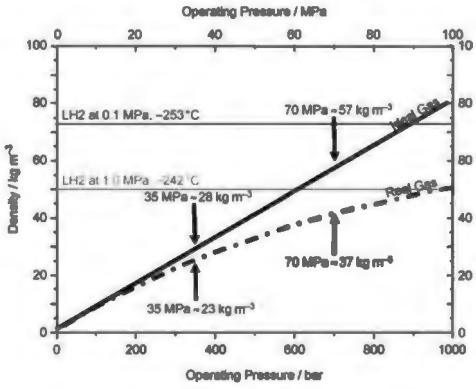

Figure 2: The density of LH2 and CGH2 systems under various conditions [5]

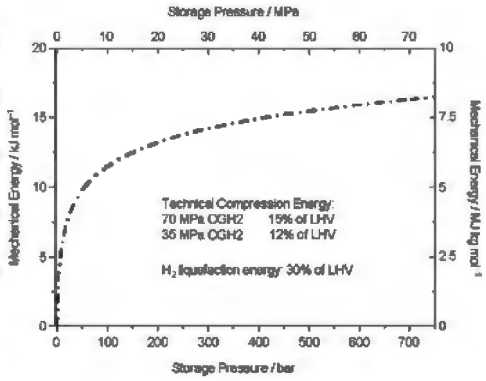

Figure 3: Mechanical energy content of hydrogen using an assumption of ideal gas and isotherm compression at 27C and constant mass [5]

The main researches on CGH_2 are concerned about the vessel: it should be light, resistant to the high pressures and hydrogen embrittlement proof.

Current CGH_2 technologies can store around 48 g H_2 per kg weight vessel [5]. Even though this gravimetric capacity does not reach the DOE targets yet, this is the closest value to them and hence CGH2 constitutes the state of the arts of hydrogen storage systems. It however remains a challenge for on board applications as integrating such high pressures in a car presents some safety issues. In Japan for example, such pressured vessels are prohibited on the roads on light duty-vehicles. Safer, more affordable and better capacity storage systems are then needed.

1.2.2. Liquid hydrogen (LH_2)

As the density of liquid hydrogen is 70.8 kg/m^3 and that of solid hydrogen 70.6 kg/m^3, storing hydrogen as a condensed phase seems appealing since the mass per container volume will increase by decreasing the temperature. However, at 1 bar, hydrogen condensates at -253 °C and its vaporization enthalpy is 452 kJ/kg. Regarding the fact that its critical point is reached at -242 °C, it must be stored in an open system in order to avoid too strong overpressure (see Figure 2) (heat transfer to the vessel would make the hydrogen evaporate readily because of the low vaporization enthalpy, leading to high overpressure). This causes huge hydrogen loss from the evaporation process, which shall be added to the loss during cooling (while refilling at hydrogen stations). These losses are difficult to minimize owing to the very low vaporization enthalpy and so far the insulating systems are not efficient enough in minimizing the heat input from the surrounding environment. Moreover, the insulation, the tank and cables are enough of heavy components to induce high density losses. The insecurity linked with LH_2 such as frostbite, the too high energy needed to liquefy hydrogen (30 % of the energy stored [5]) along with those hydrogen and density losses, hinder its use as on-board hydrogen storage system as no strong advantage which would compensate these drawbacks appears.

1.2.3. Solid state hydrogen storage

Regarding the extreme pressures and temperatures used for CGH_2 and LH_2 respectively, more practical alternatives for on-board applications have been investigated. Due to its high gravimetric storage and rapid refueling time, CGH_2 remains the state of the arts, but using a host material as a hydrogen carrier has emerged as a promising mean. Solid state hydrogen storage refers to two kinds of materials: those which trap molecular hydrogen in their pores via physisorption, the heat of enthalpy is typically around 4~7 kJ/mol; and those which dissociate hydrogen and bind strongly with each atom via chemisorption with a heat of adsorption greater than 20 kJ/mol.

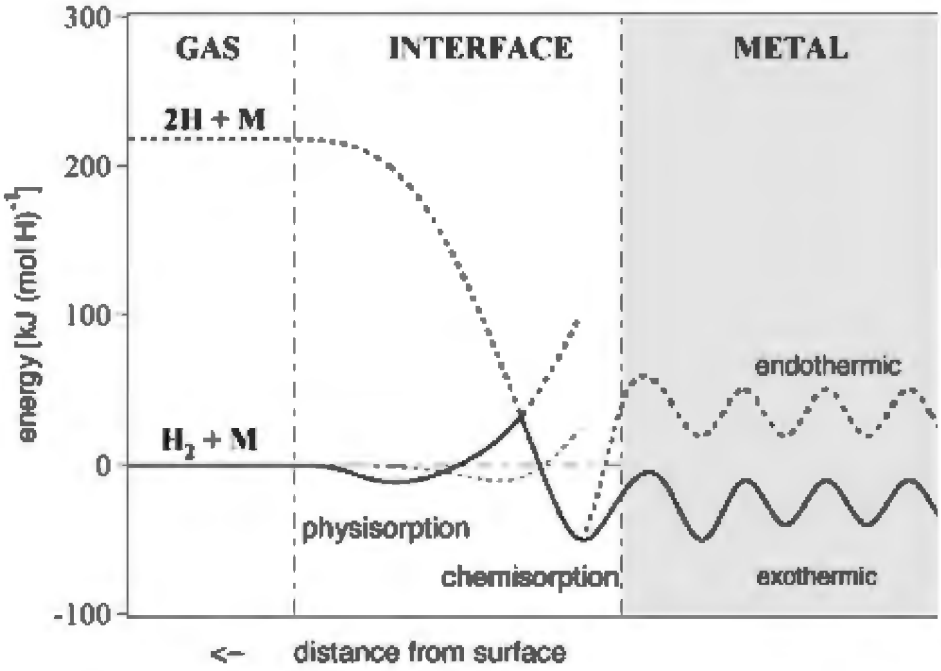

Figure 4: Scheme of potential energy curves of hydrogen in molecular and atomic form approaching a material. The hydrogen molecule is attracted by Van der Waals forces and form a physical physisorbed state. In case the material is a metal, chemisorption will occur [6].

1.2.3.1. Chemisorptive storage materials

Chemisorptive storage materials refer commonly to hydrides, which are binary compounds between hydrogen and other elements of the periodic table. They can be simple metal hydrides, reversible complex metal hydrides or irreversible chemical hydrides.

1.2.3.1.a. Simple metal hydrides

Simple metal hydrides are binary metal hydrogen compounds with a formula MH_x where M represents a metal. For gravimetric considerations, lightweight materials, such as alkali and alkaline earth

metals, suit the best for hydrogen storage. Owing to the larger electronegativity of hydrogen, this one shares an ionic bond with the lightweight metal, but in the case of transition metal (more rarely used) the bond is rather metallic or interstitial. The release of hydrogen requires a decrease in pressure or increase in temperature.

Lithium hydride (LiH), the simplest and lightest metal hydride, stores up to 12.6 wt% H_2 at room temperature [7]. The release of hydrogen occurs however only at high temperature (> 1000 K) and the kinetics are too sluggish [8] to consider it as a candidate for hydrogen storage. Other simple hydrides (NaH, MgH) decompose at lower temperature (< 700 K), together with lower hydrogen contents, but the kinetics remain too slow here too (release within days).

These hydrides, even if they reach the gravimetric targets for the most of them, release the hydrogen so slowly that they are considered non-reversible for the relevant temperature and pressure ranges. Researches to foster the kinetics focus on size reduction to synthesize nanoscale powders [9] or thin film metal hydrides [10].

1.2.3.1.b. Reversible complex metal hydrides

Complex metal hydrides are made of hydrogen covalently bound to a central atom in an anion complex (e.g. $[AlH_4]^-$, $[BH_4]^-$, $[NH_2]^-$) stabilized by a cation (alkali, alkaline earth or transition metal). Here too, gravimetric considerations favor the use of light elements (Z≤13).

They are called reversible because they can uptake hydrogen and release a non-negligible amount of the stored gas in the reverse reaction in a certain range of pressures and temperatures. The discovery of their reversibility, compared to simple hydrides, constituted a breakthrough in solid state hydrogen storage. Complex hydrides studied in the context of hydrogen storage refer to three categories: alanates, borohydrites and amides.

Alanates are hexahydroaluminates (Al octahedrally coordinated by H) or tetrahydroaluminates (Al tetrahedrally coordinated by H).anion complexes bound to a cation. Sodium alanate ($NaAlH_4$) can release 4 wt. % H_2 at 160 °C [11]. The kinetics remain however sluggish. These alanates are especially interesting for their low temperature reversibility.

Borohydrites are composed of brome and hydrogen anion complexes. Alkali borohydrides have been the most studied. They show a better hydrogen content than alanates but are thermally too stable and hence require high temperature to desorb the gas stored [3]. Lithium borohydride for example stores up to 13.5 wt. % hydrogen but decomposes only at temperatures higher than 270 °C [12]. They present also slightly more kinetics issues than the alanates [3].

Amides are nitrogen-based hydrides that have received much attention for hydrogen storage. They usually react with lithium hydride to decompose and release hydrogen. For example, the reaction between

lithium amide ($LiNH_2$) and lithium hydride leads a theoretical capacity of 10.3 wt. % at temperatures greater than 400 °C [13]. The main problem of amides resides in the possible ammonia (NH_3) production and the loss of nitrogen degrades the material what leads to a lower performance cycle after cycle.

Even if these complex hydrides fulfill some of the targets for hydrogen storage, none of them meet the capacity, thermodynamic and kinetics requirements at the same time. Current research are then focused on fostering the kinetics by reducing their size in the nanoscale, and on tailoring the thermodynamics by alloying and hybridizing them [6, 10, 14-16]

The main drawback that hinders their use in light duty vehicle remains yet the heat management while refueling. Indeed it is a very endothermic process, what explains their high stability and the high temperature needed for decomposition. On-board hydrogenation is more likely to damage some components and particularly to cause huge energy waste.

1.2.3.1.c. Irreversible chemical hydrides

As can be inferred from their names, the thermodynamics and/or kinetics do not favor facile hydrogenation once decomposition occurs. The decomposition process alters the original material in such a way that on-board refueling cannot occur. They have however been

investigated as promising hydrogen storage materials because some of them present faster kinetics and decompose at lower temperature than complex hydrides.

One good example is aluminum hydride which decomposes into aluminum and hydrogen, which has a gravimetric capacity greater than 10 wt. %, decomposes at temperatures lower than 100 °C [17] at fast rates. The crystallographic phase changes [18] between the hydride and the metal form imposes however a single use and hydrogenation can occur again only off-board and after retreatment of the metal.

Main current researches focus then on controlling the decomposition and regeneration processes so that on-board refueling, main shortcoming of these hydrides, could take place.

1.2.3.2. Physisorptive materials

Contrary to hydrides in which hydrogen atoms are strongly bound to the element via ionic, covalent or interstitial bound, in physisorptive materials, weak Van der Walls forces take place as illustrated in Figure 5. The uptake is ruled by Van der Waals forces between the hydrogen molecule and the surface of the adsorbent, and given the physical properties of hydrogen, only a monolayer can be adsorbed at temperatures higher than its boiling point (-252 °C) [19], so that higher

amounts are stored only at lower temperature. The hydrogen uptake depends then mainly on:

- (1) The textural characteristics of the surface: higher surface areas allow higher hydrogen uptake by physisorption because of a higher density of binding sites. Moreover, the size and diameter of the pores play an important role as capillary condensation can also occur. Pores classification fall into three groups: macropores with an average pore diameter exceeding 50 nm, mesopores with an average pore diameter comprised between 2 and 50 nm and micropores with an average pore diameter smaller than 20nm, which can be further divided into super-micropores (0.7 – 2 nm) and ultra-micropores (<0.7 nm). So given the kinetic diameter of the hydrogen molecule (2.89 Å), the adsorption potential on the pore walls of smaller pores will overlap leading to a higher adsorption energy [20]. The predominance of microporosity yields then to a higher hydrogen uptake.
- (2) The enthalpy of adsorption: the adsorption enthalpy of physisorption is not higher than 10 kJ/mol (smaller values for carbon materials and higher ones for other organic materials).

Requirements of high specific surface area (SSA), high micropores volume and high adsorption enthalpy made high SSA carbonaceous

materials, in which the physisorption enthalpy values around 2-7 kJ/mol, good candidates for hydrogen storage. They have mostly been investigated for adsorption at liquid-nitrogen temperature (77 K) and ambient pressure but more and more researches are being done on room temperature adsorption and pressures up to 10 MPa. The following discussion will only deal with progress made on room temperature hydrogen storage, condition closer to the U.S. DOE targets.

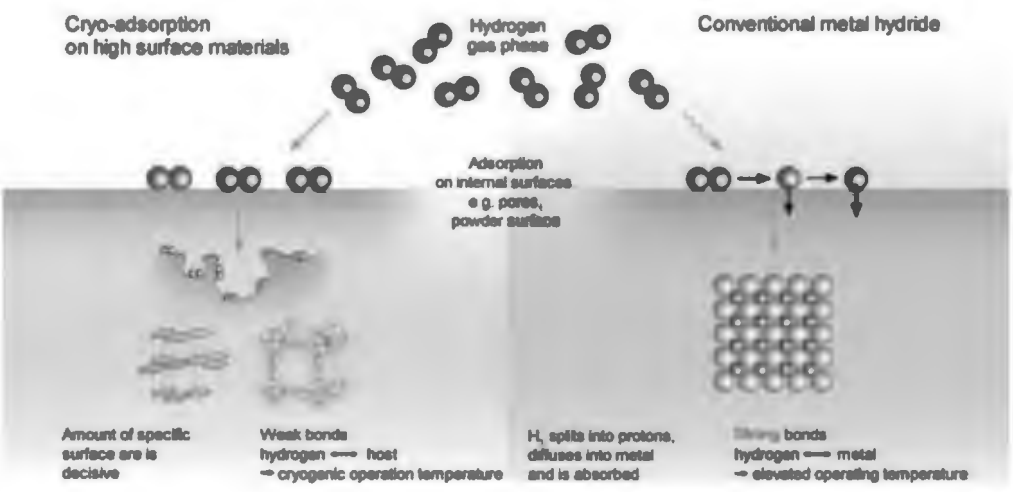

Figure 5: Representation of cryoadsorption and chemical storage in a hydride [5]

Materials which can uptake hydrogen via physidorption are really interesting because they are carbonaceous, and hence lightweight, can be mass produced from a variety of precursors, have a good SSA and pore volume, and more importantly, can uptake and release hydrogen without suffering from the harsh conditions predominant upon previous

storage means (high pressures, liquid hydrogen temperature or too high temperature, slow kinetics).

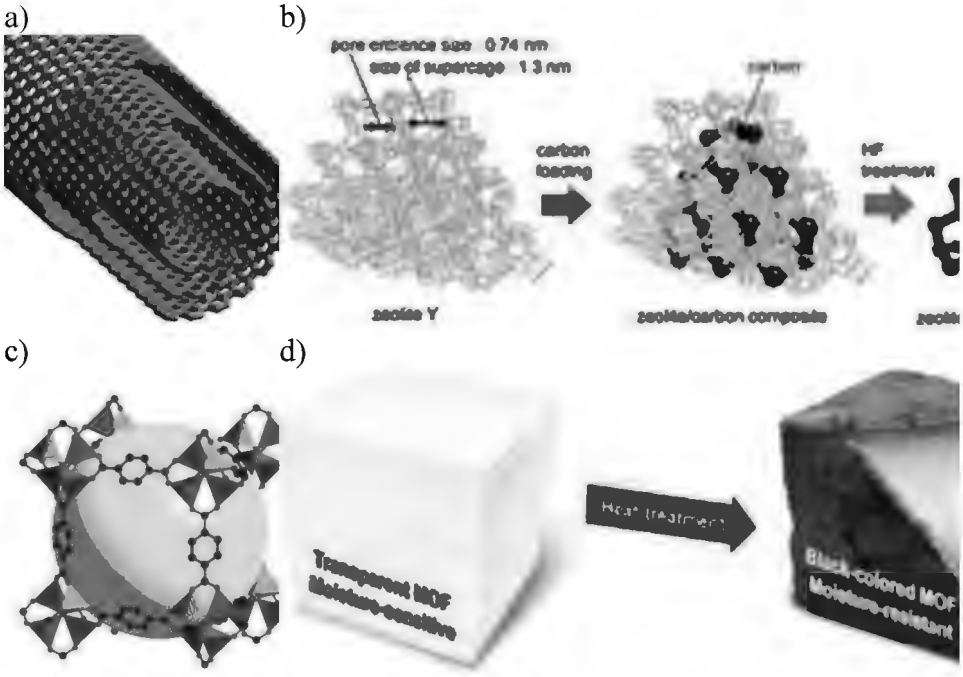

Figure 6: Various hydrogen storage materials: a)MWCNTs, b)ZTCs, c) MOF, d) to MDC synthesis

The main of them (see Figure 6) are activated carbons (Acs), zeolite-template carbons (ZTCs), metal-organic frameworks (MOFs), MOF-derived carbons (MDCs) and carbon nanomaterials such as carbons nanotubes (CNTs) which somehow opened the road to the numerous investigations upon physisorptive materials. Indeed, Dillon et al. [21] and Chambers et al. [22] reported an uptake of 10 wt. % and 67 wt. % at room temperature in single walled CNTs (SWCNTs) and graphite nanofibers respectively. The non-reproducibility of these results in the

following years (Figure 7) brought to the conclusion that more than 1 wt. % room temperature hydrogen storage in carbon nanomaterials is erroneous and merely due to experimental errors.

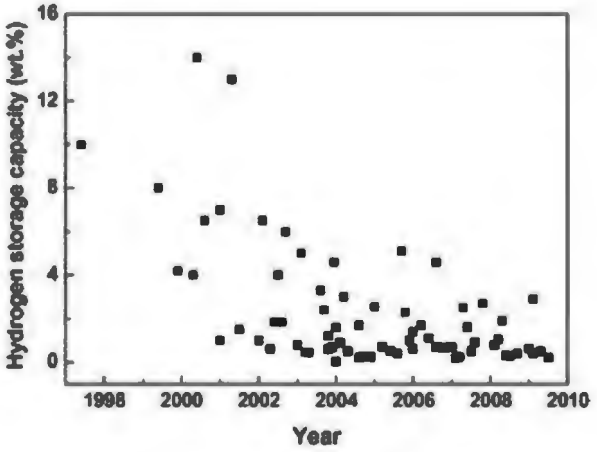

Figure 7: A plot of the reported hydrogen storage capacities of CNTs from the literature versus their year of publication [23].

All along the researches in these materials, it appeared that their porosity texture (pores shape and distribution) governs the uptake of hydrogen. This uptake also increases with increasing SSA materials as shown in Figure 8.

The knowledge of such dependency opened the road to the design of materials with high SSA and predominant microporosity for room temperature hydrogen storage. ACs are highly porous and can be synthesized from various organic precursors as well as agricultural wastes (e.g. an apple core), what makes them amenable to large scale preparation. Jorda-Beneyto et al. [24] synthesized an AC, KUA5, with

a 3183 m^2/g BET SSA and 1.27 cm^3/g microporosity, which exhibited 0.8 wt .% H_2 at 100 bar.

Knowing the importance of microporosity and the high disordered pore structure in ACs, ZTCs appeared as an alternative with ordered regular porosity. They are obtained through templating methods by (1) incorporating carbon precursors in zeolites (which are microporous alumino-sillicate polymers) through chemical vapor deposition or liquid impregnation, (2)carbonizing the obtained material (3) and washing out the zeolite framework through successive washing with strong acids. Nishihara et al. [25] reported 0.87 wt% H_2 uptake, at room temperature and 10 MPa, in a ZTC with a high BET SSA of 3300 m^2/g and uniform microporosity with a diameter of 1.2 nm.

Metal organic frameworks have also received tremendous attention due to their high SSA and tunable porosity. MOFs are crystalline materials built up from metal clusters or ions (called single building units (SBU) linked with organic ligands, creating that way a network of pores and channels. Various MOFs, whose properties depend on the SBUs and ligands chosen, have been reported. They exhibit the highest surface area up to date _7140 m^2/g for NU-110E born from the solvothermal reaction between hexa-carboxylic acid and copper nitrate tetrahydrate [26]_ and their porosity can be finely tuned by the choice of the linker. Since the work of Rosi et al. [27] who reported the first study on

hydrogen uptake into MOFs (MOF-5), a plethora of works followed, well reviewed by [4, 28-33]. One of the most interesting ones remains the isoreticular MOF, IRMOF-1, which uptakes up to 0.45 wt. % H_2 at room temperature and 100 bar, with a 3440 m2/g BET SSA [34], see Figure 8.

Following the example of ZTCs, MOFs also have been used as template for carbon materials. MDCs can be synthesized either by following the same procedure than ZTCs, or by merely carbonizing the metal organic framework until evaporation of all non-carbonaceous components. Because they derived directly from MOFs, a well-controlled carbonization process could induce a limited loss in SSA and porosity so that MDCs have good textural characteristics approaching that of MOFs, besides their light weight. Only few MDCs have been investigated since the pioneer work of Yang et al. [35] who carbonized an IRMOF-1 structure and obtained a MDC-1 showing up a BET SSA of 3174 m^2/g and a hydrogen storage capacity of 0.94 wt.%, the highest reproducible uptake ever reported for carbonaceous materials at 298 K and 10 MPa.

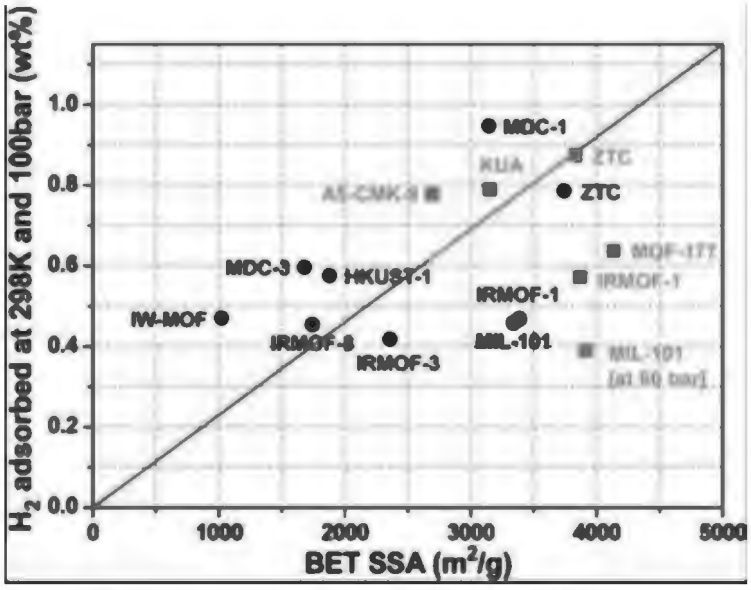

Figure 8: H2 storage capacities at 298 K and 100 bar for various ultrahigh porous carbons and MOFs plotted as a function of the BET SSA [34].

Other adsorbents such as zeolites or carbide-derived carbons have also been investigated, less deeply though. However, even if all the adsorbents store a non-negligible amount of hydrogen at room temperature and release it within minutes under milder conditions than previously presented storage systems, they still absorb less than 1 wt. % H_2, amount which lays quite far below the U.S. DOE targets. Efforts have then been put on trying to improve the sorption capacity of these adsorbents.

1.3. Tailoring hydrogen uptake in physisorptive materials

1.3.1. Introduction

As stated previously, the adsorption in high SSA materials leans on the SSA, the pores volume and the adsorption enthalpy. Despite the high SSA and micropores volumes reported for some materials (such as MOFs whose SSA can hypothetically reach 14600 m^2/g [26]), the stored amount does not seem to exceed 1 wt. % H_2. New strategies are then needed and these are mostly focused on tailoring the heat of adsorption. Theoretical studies on optimum conditions for hydrogen storage have shown that the heat of adsorption should be drastically increased up to 15.1 KJ/mol [36] in order for the adsorbent to accuse an acceptable storage capacity at room temperature and under a delivery pressure of around 1.5 bar.

Strategies to increase the heat of enthalpy, and by the same way the stored hydrogen, mostly depend on the adsorbent itself. MOFs for example were the most studied in that way because their tunable SSA, porosity, ligands functionalities and metal building unit leave rooms for so many applications (e.g. ligands functionalization, other metal incorporation) [32].

One strategy that has however shown its fruits for almost all currently studied porous sorbents remains their hybridization by transition metal doping.

1.3.2. Transition metal doping: promoting spillover

The importance of metal doping for hydrogen storage at room temperature appeared with Lueking and Yang [37] who reported enhanced hydrogen storage in multiwalled carbon nanotubes (MWCNTs) with residual metal catalysts. Indeed, metal oxide catalysts were used for the synthesis of MWCNTs, and then washed out to purify the CNTs. When the acid washing is not effective, some metal oxide catalysts ($Ni_{0.4}Mg_{0.6}O$ in their work) remain on the surface of the carbon nanomaterials and hydrogen sorption measurements on those residual metal oxides - containing MWCNTs revealed an uptake of 0.65 wt. % compared to a non-measurable uptake in the case of well washed metal nanotubes. They then concluded that the metal oxides played a role in the adsorption of hydrogen. A further investigation of the uptake of the bare metal catalysts showed that the great enhancement cannot be only imputed to the metal oxide catalyst, suggesting a common participation of both the carbon adsorbent and the catalysts. Moreover, temperature programmed desorption (TPD) measurements gave an activation energy of desorption of 97 kJ/mol for

the catalyst-doped carbon adsorbent (value too high to suggest physisorption), compared to 115 kJ/mol for the bare catalyst, suggesting that the hydrogen is more loosely bound to the catalyst-adsorbent system. Lueking and Yang explained then their enhancement in the terms of spillover: primary dissociation of the hydrogen molecule on the surface of the metal catalyst, followed by a "spillover" onto the adsorbent plus further diffusion.

Spillover of hydrogen was not new and had been reported decades ago [38-41] and its possible use in hydrogen storage was proposed some years before Lueking and Yang's work in a U.S. patent [42], but its effectiveness in hydrogen storage at room temperature in carbonaceous materials was a novelty. The conclusion of the authors about the mechanism ruling the enhanced hydrogen uptake was also comforted by a previous work of Yang et al. [43] in which ab initio molecular orbital studies showed that hydrogen spillover onto a graphite support was possible and bonding of hydrogen atoms on basal plans was exothermic and then stable at room temperature.

1.3.3. Hydrogen spillover

Spillover is a general phenomenon defined by "the transport of active species adsorbed or formed on a first surface onto another surface that

does not under the same conditions adsorb or form the active species" [44].

The spillover of hydrogen has been intensively used in catalyst field and refers to three processes (see Figure 9): (1) chemisorptive dissociation of hydrogen onto a metal (or metal oxide) catalyst, (2) migration of the dissociated hydrogen atoms onto the support of the catalyst and (3) diffusion into (or onto) that support.

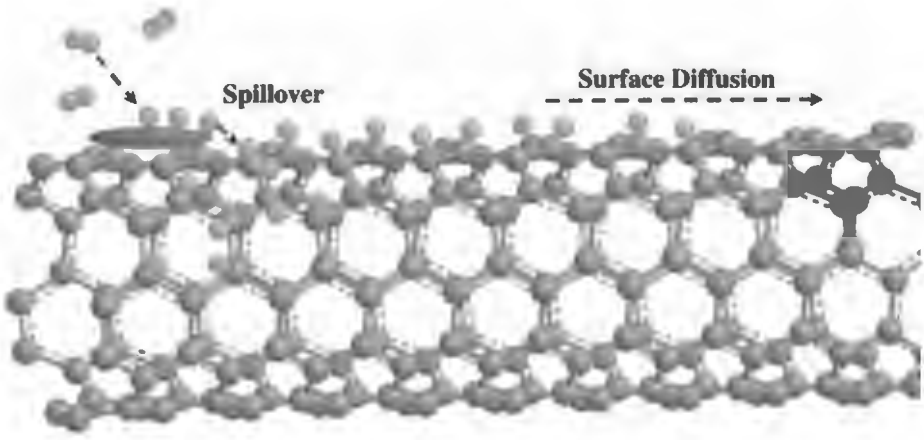

Figure 9: Hydrogen spillover includes dissociative chemisorption of hydrogen on metal nano-particles and subsequent migration of hydrogen atoms onto adjacent surfaces of a sorbent (e.g. single walled carbon nanotube) via spillover and surface diffusion [45].

In 1964, Khoobiar [38] gave the first experimental evidence of this phenomenon. Hydrogen atoms normally reduces tungsten trioxide (WO_3, basically yellow) at above 200 °C (and not room temperature) to give a blue oxide. A mixture of WO_3 with a platinum-supported aluminum oxide catalyst was passed under a hydrogen flow at room temperature. The yellow tungsten oxide turned to blue, suggesting a

dissociation of hydrogen molecule on Pt followed by the migration of the H atoms to WO_3.

Subsequently, interest has been led upon that phenomenon. Scientists have tried to bring a scientific proof to the mechanism behind spillover. It was stated that actually, H atoms do not migrate, but protons and electrons do, and they do migrate only to a reducible support [46]. Spillover to a non-reducible defect-free surface (such as carbon surfaces) was believed improbable, but recent advances on hydrogen storage showed that it might be possible onto graphitic surfaces. Indeed, Schwarz [42] proposed an increase in the hydrogen uptake by spillover at cryogenic temperature (and not room temperature), and Srinivas [40] observed a direct evidence of spillover from platinum to its carbon support through the hydrogenation of benzene.

1.3.4. Hydrogen spillover in the context of hydrogen storage in carbonaceous materials

After Lueking and Yang reported their enhancement [37] obtained from hydrogen spillover, a subsequent number of studies claiming an increased uptake by spillover has arisen on almost all carbonaceous materials previously cited.

Carbon nanotubes have been the most studied for hydrogen storage (with and without metal doping) among carbon nanomaterials (e.g.

single and multiwalled carbon nanotubes (SWCNTs and MWCNTs), carbon nanofibers, graphene). Lueking and Yang realized a systematic investigation of various carbon materials in order to check if the amount stored would increase after platinum and palladium doping [47]. As can be seen in Figure 10 which shows the uptake for various Pd-doped carbon materials (Pd/Arc R, Pd/SW 5R and Pd/MW (5R)) compared to their non-doped counterparts respectively (a multiwalled CNT MWNT, a single walled CNT SWNT, an activated carbon Arc HT AX21) and to a commercial Pd-supported carbon catalyst (PdC 5% 1890). In each case, a clear enhancement appeared, what the authors explained with hydrogen spillover occurrence.

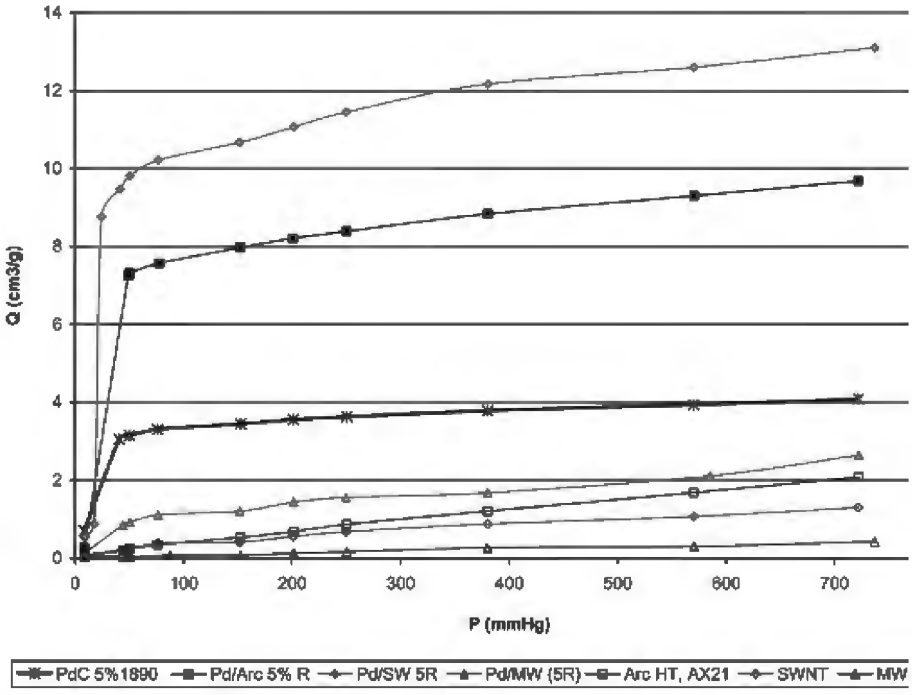

Figure 10: Hydrogen uptake for different primary metal-carbon systems compared to the corresponding non-doped carbons [47]

They also noticed that mixing the doped carbon materials with non-doped ones further increased the hydrogen uptake and explained this phenomenon by secondary spillover (Figure 11). It was said that secondary spillover reduced the number of experimental variables, allowed to isolate the properties of the secondary carbon which accepted the spilt-over hydrogen atoms, dispensed from taking into account the efficiency of metal doping, the dispersion and the carbon/metal interface which are important parameters for the primary carbon.

The increase in the amount of stored hydrogen constituted, for the authors, a sufficient proof that hydrogen spillover did occur and that atomic hydrogen was stored in the final receptor. Moreover, no reversibility was discussed in their work.

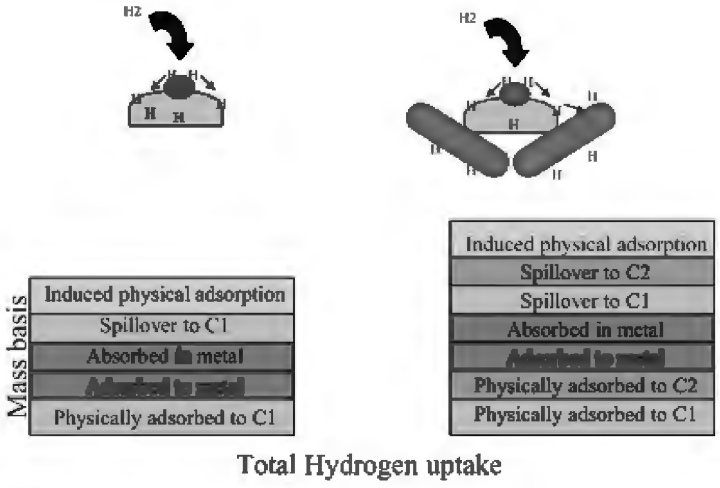

Figure 11: Schematic comparing primary to secondary spillover and how each component contributes to overall hydrogen uptake. C1 = primary carbon, C2 = secondary carbon

Apart from carbon nanomaterials, MOFs have also been intensively studied, particularly by R. T. Yang and coworkers [43, 48-52]. By physically mixing Pt-supported on activated carbon catalyst with two isoreticular MOFs (IRMOF-1 _also called MOF-5_ and IRMOF-8), they managed to obtain an enhancement **factor** of 3.2 and 3 for MOF-5 and IRMOF-8 respectively [48]. Here again, the enhancement was attributed to secondary spillover (primary spillover taking place between the platinum and the activated carbon). By putting carbon bridges, better enhancement factors (7.8 and 8 for MOF-5 and IRMOF-

1 respectively) suggested that additional bridges allowed more intimate contact between the source and the support, hence reducing the activation energy barrier for popping from a surface up to another (Figure 12). The hydrogen uptake was totally reversible and belongs among the highest in the literature. However, other groups could not yet validate such high performance of the Pt/AC/MOF composites, and some of them (Campesi and coworkers [53]) strongly denied the work of Yang et al., leading to lively responses between both groups.

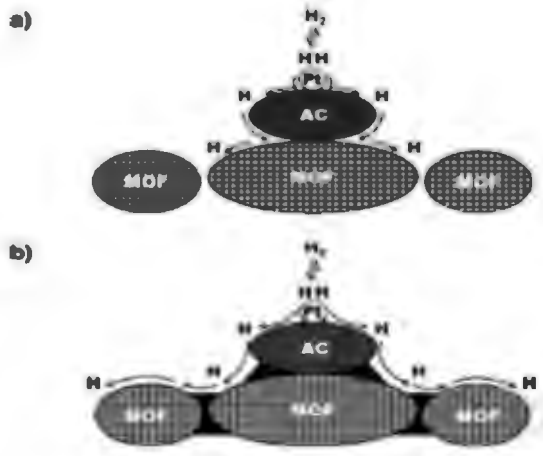

Figure 12: (a) Primary spillover of atomic hydrogen from the Pt metal to the AC support and secondary spillover to the MOF receptor that has limited contacts with the support. (b) Facilitated primary and secondary spillover by using carbon bridges [49].

Because the simple mixing of MOFs and catalysts (by mortar grinding or milling) could significantly damage the texture (SSA and pores volume) of the MOFs, metal-supported carbon-doped MOFs materials obtained in situ during the MOFs solvothermal synthesis have been reported too. So the Pt loaded at CNT in MOF-5 hybrid composite

material from S. J. Yang's group [54] stores up to 1.25 wt. % H_2 at room temperature and 100 bar (corresponding to an enhancement factor of 2.7) and the Pt-doped graphene oxide/MIL-101 _ a MOF with chromium as building unit_ from Yuan's group up to 0.75 wt. % H_2 (corresponding to an enhancement factor of 1.8 %). However, the reversibility was not checked, or at least published, in any of these reports.

In parallel to these groups who showed a gain in hydrogen uptake with total reversibility (be it shown in their paper [50] or not [55]) or with a non-studied reversibility, other groups reported a non-reversibility. Campesi et al. [53], while investigating the same material reported by R. T. Yang et al. [49] (i.e. the Pt-doped activated carbon mixed with MOF-5 and bridged with sucrose), noticed a timid enhancement for the bridged material and no enhancement at all for the unbridged one. This implies that no spillover occurred and the hydrogen was adsorbed into the platinum particles, or if spillover occurred, the spilt-over hydrogen chemisorptively bound the carbon surface and hence was too stable to get released.

Numerous of other hybrid and composite materials have been investigated [45, 46, 56, 57]. Figure 13 shows results which are among the best reported for carbonaceous materials. Some of them showed a great enhancement as reported above while others (a small part of the

reports) did not suggest any benefit in doping with transition metal particles. In most of the studies which noticed an increased uptake, it was explained through spillover, without actually giving any other proof than the enhancement itself. Spilt-over hydrogen atom is hard to detect directly due to the nature of the hydrogen atom itself which is the smallest chemical element. Moreover, the spillover mechanism in hydrogen storage remains a mystery despite all numerical studies based on density functional theories (DFT) which tried to explain it. So the authors linked their enhancement to spillover. However other processes (such as a simple chemisorptive absorption by the metal particle) could also occur; and without adsorption enthalpies calculations (to detect physisorption, chemisorption or something in between), reversibility determination (to check if all adsorbed hydrogen can be released at room temperature), kinetics recording (to verify how feasible such synthesized system could be in on board applications) and spillover analysis itself if possible (using inelastic neutron scattering _INS, even though one could easily understand that such technique is not affordable), we cannot easily attribute the increase in hydrogen stored to spillover. The best that can be done is to understand that the hybrid formation changed in a way the physicochemical properties of the pristine adsorbent, the true mechanism behind it being till now unknown.

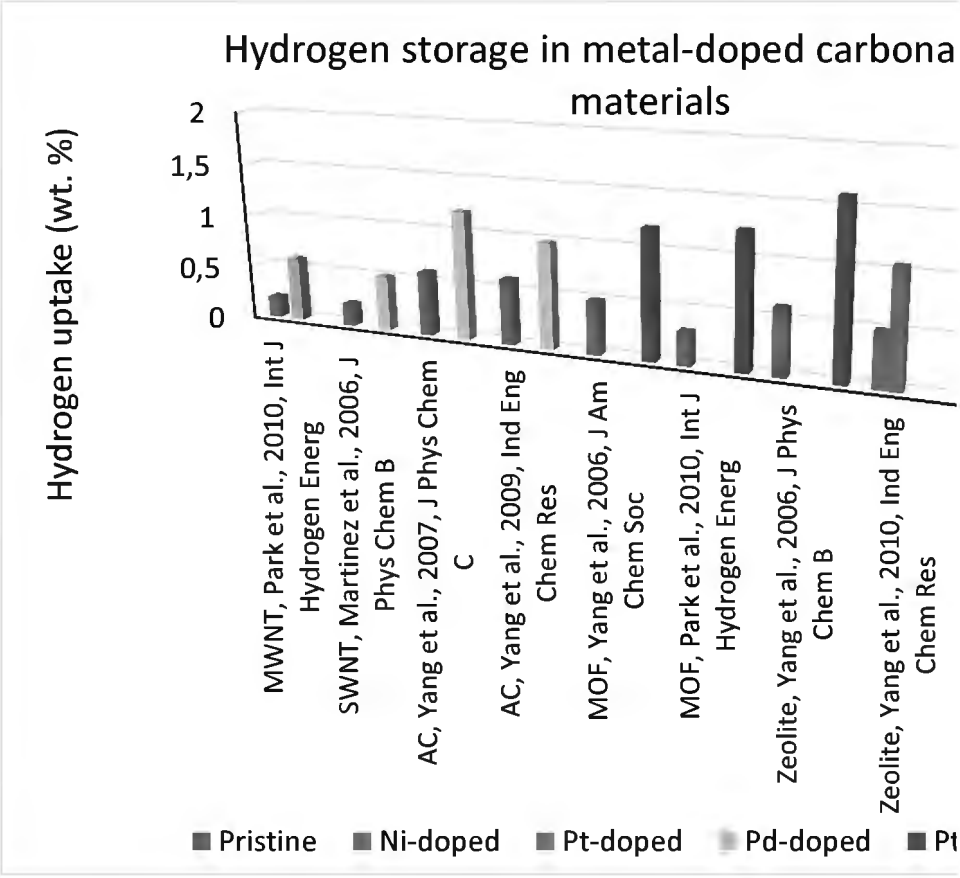

Figure 13: Hydrogen storage in various metal doped carbonaceous materials

Some scientists have however attempted to give a concrete proof about spillover when it comes to hydrogen storage.

1.3.5. Experimental study of hydrogen spillover for hydrogen storage

Basically two main ways can detect spilt-over hydrogen. One is the electronic or chemical state change of the material that welcomes the atomic hydrogen. The reduction of tungsten oxide [38], easily noticed by color changing, and the hydrogenation of benzene [40] are proofs of

the adsorption of atomic hydrogen. The other one consists of measuring directly (experimental proof) the dynamics of atomic hydrogen on the support. In fact, obtaining a direct proof is challenging. Up to now, small transition metal particles have been used along with a carbon support to study the hydrogen uptake by spillover. The use of Raman or IR spectroscopy is limited by the adsorption of electromagnetic radiations by small metal particles and carbon. Moreover, magnetic resonance cannot be used due to the electrical conductivity of carbon [58] and X-ray techniques are not enough powerful to explore hydrogen at an atomic scale [59]. Neutron scattering methods however are efficient because of the high incoherent cross section energy of hydrogen (80.26 barn) _see Figure 14.

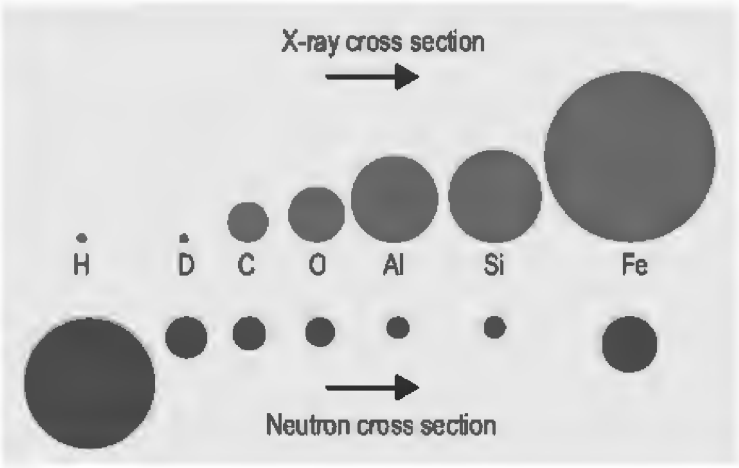

Figure 14: X-ray and neutron scattering cross section comparison

Inelastic neutron scattering has proven itself to be a powerful tool to detect spilt-over hydrogen on carbon supported fuel cell catalysts.

Contescu et al. [58] therefore used it in order to prove experimentally that spillover was responsible for the increase in hydrogen uptake in metal particle-doped porous materials for hydrogen storage at room temperature. In their study, palladium (Pd) was doped onto activated carbon fiber (ACF) and the as obtained Pd-ACF was inspected by INS. The observation of C-H peaks at the experimental conditions (20°C, ambient pressure), coupled with the knowledge that non-catalytic hydrogenation of graphite is not probable at these conditions, confirmed that atomic hydrogen spilt-over from the metal catalyst and reacted with the carbon surface to form stable C-H bonds. Their system also showed a slight irreversibility and the chemisorbed hydrogen could not be released, even at temperatures greater than 300°C. The irreversible amount was yet still small compared to the overall increase of stored hydrogen, meaning that some of the spilt-over hydrogen was stored reversible.

That study, as well as other ones that dealt with hydrogen spillover in activated carbon-based hybrid [59] or MOF-based hybrid [60], gave a clear statement of the presence of spilt-over hydrogen atoms on the surface of the receptor, some of them binding irreversibly to the carbon (in case of carbon materials) or to the functional groups (in case of MOFs). Such experimental set up (INS) can however not be used for all works related to hydrogen storage using spillover because of its non-

affordability, but as these studies were effective in showing spilt-over hydrogen, one can more easily agree with those who claimed big increased in hydrogen uptake due to spillover (see page 25).

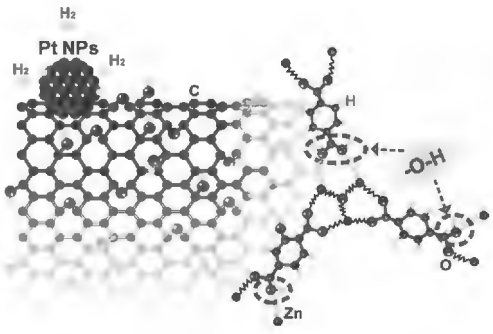

Figure 15: Hydrogen spillover from Pt nanoparticle to a carbon support, binding to functional groups [60]

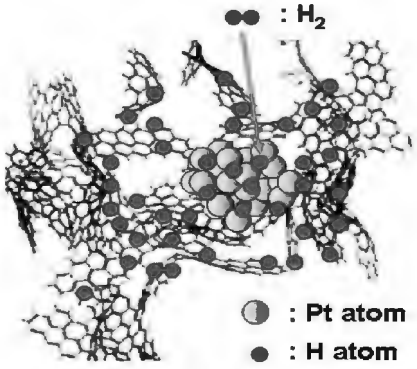

Figure 16: Hydrogen spillover from Pt nanoparticle to a carbon support, binding to carbon [61]

Being able to detect spillover partly unveils the phenomenon that is behind the uptake enhancement and the irreversibility noticed for some materials, but it still does not give a full understanding of it. The whole mechanistic, kinetics and thermodynamics behind are still unknown, what explains why results are inconsistent from a group to another.

1.3.6. Spillover mechanism in hydrogen storage

The experimental results proving spillover constitute a clear statement that spillover occurred at room temperature and favors the storage of hydrogen in some carbonaceous materials. This does not seem to be a

questionable point. The mechanism remains however obscure and few attempts gave a comprehensive understanding of the machinery lying behind spillover.

The most interesting and plausible one remains the one proposed by Psofogiannakis and Froudakis [62] who went through the experimental reports of hydrogen spillover, the direct experimental proofs and the theoretical simulations about spillover from metal catalyst to graphitic materials and MOFs; and came up with a model.

When it comes to spillover, Pt and Pd particles have been the most used because (1) they do not bind hydrogen as strongly as the alkali, earth-alkaline or other transition metal, (2) they prove their efficiency in the catalyst field and (3) they are known to promote hydrogen spillover.

According to their study, hydrogen approaches first the surface of the metal particle, which dissociates it readily at room temperature and binds it more or less strongly, before pumping it to the support. Indeed, during the dissociation process, one of the atoms at least gains enough kinetic energy to get ejected in the gas phase. This gas phase atom generation could originate from the temperature, the pressure of hydrogen molecules, the shape, size or state of the nanoparticles, but the role of these parameters is not understood yet.

The as unbound hydrogen having a short life cycle, it quickly reacts with the support surrounding the metal particle, before entering either a

physisorbed state or a chemisorbed one (see Figure 17). Both states have been directly observed using INS and their energy measured with density functional theory (DFT) calculations.

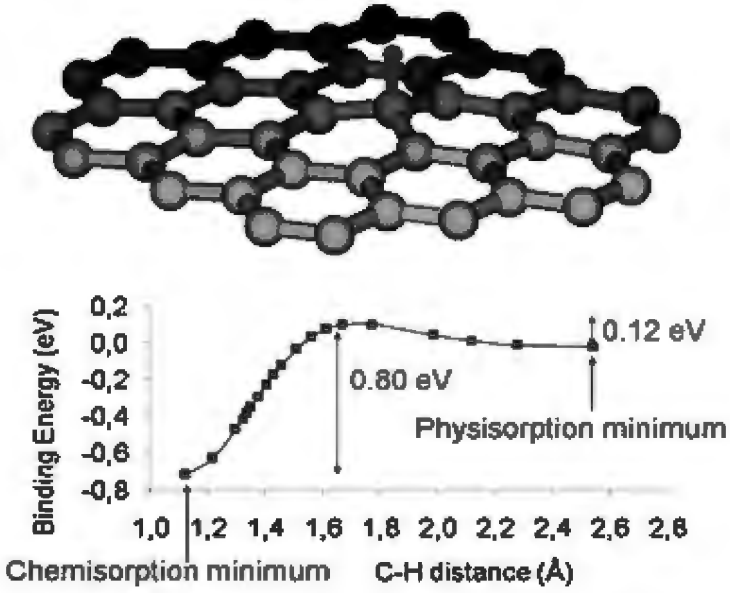

Figure 17: "Top: Structure of a chemisorbed H atom on graphene. Bottom: The diagram shows the dispersion-corrected DFT interaction energy of a single H atom with a graphitic surface, as a function of the C–H bond length. The interaction is characterized by the strong chemisorption and weak physisorption minima" [62]

When trapped in a physisorption well, atomic hydrogen can diffuse on the graphitic surface until chemisorptive recombination with a sp^2 carbon, new spillover to a new surface (in that case a small energy barrier need to be overcome) or desorption in the gas phase and recombination with another hydrogen atom. This explains why reversible hydrogen storage, secondary spillover and irreversible hydrogen storage are likely to happen. When hydrogen is in the gas phase, because of its instability, it can easily migrate to other sites or

surface or recombine with another atom on the surface. This can explain the diffusion process in spillover.

Hydrogen atoms moving freely on a graphitic surface (getting trapped in a physisorbed state, then diffusing in the gas phase, then getting trapped again, and so on) are however limited and more stable chemisorption wells can thus be occupied.

The equilibrium conditions _relative concentration of hydrogen atoms in the physisorbed state, the chemisorbed state and the gas phase_ are still not well known and might depend on the temperature, the pressure, the defects on the support and its purity (presence of oxides).

This model gives an insight of a possible mechanism, based on the review of publications dealing with spillover. Even if it does not fully describe the mechanism, it however is in accordance with the majority of the reports so far and even gives reasons for their discrepancies.

Other model [50] also tried to explain the mechanism of hydrogen spillover in hydrogen storage, but this was more based on the only works of that research group and then fails to describe other studies.

1.4. Scope, purpose and value of this study

1.4.1. Limitations of previous works

Compared to compressed gaseous hydrogen and liquid hydrogen, solid state hydrogen storage is safer and more compact, making it more

suitable for on-board application. Besides, storing hydrogen in porous carbonaceous materials can be achieved at mild conditions and fast kinetics, what helps get rid of the harsh temperatures and sluggish kinetics in the hydrides systems. Porous materials do not however store significant amount of hydrogen at room temperature, unless they are doped with other materials/chemical elements in order to foster the heat of enthalpy governing the physisorption that takes place.

Doping with metal catalyst has proven its efficiency in increasing the quantity of hydrogen that is effectively stored in a porous material. Spillover seems to explain such enhancement as spilt-over hydrogen has been detected on the particle support, and spillover is so far the only phenomenon that manages to give a clue about the increase in hydrogen uptake. Reports in the literature remain however contradictory. While some groups manage to find a totally reversible enhancement, other groups reported an irreversible one, other no enhancement at all, and few researchers even reported a decrease in the hydrogen uptake.

Such discrepancies might have various causes, the more important of which being the total lack of understanding of mechanism, kinetics and thermodynamics that govern spillover. The useful and optimum parameters that lead to spillover are till yet unknown (e.g. temperature, pressure, particle size shape and distribution, material texture). As it

appears challenging to fully follow hydrogen atoms in spillover and separate the kinetics and thermodynamics governing the storage of hydrogen, a way of proposing a mechanism seems to be by investigating a number of materials and learn from the differences or similarities.

A plethora of materials have been investigated. We could expect that once spillover has proven its efficiency, materials which show the highest uptake at room temperature would be explored too, but quite surprisingly, no research questioned yet the possible uptake when hybridizing MDC with transition metals. When we look through hydrogen storage in carbon nanotubes, at 10 MPa, the hydrogen stored after transition metal doping is lower than 0.6 wt. % [54] while the pristine MDC can store up to 0.94 wt. % [35].

Besides, previous works usually did not focus on the transition metal used for hybridization. In a catalyst point of view, it is known that the particle size has to be the smallest possible because catalyzing a reaction is a surface phenomenon and the highest the surface area (or the smallest the particles), the highest the catalytic power. Wang et al. were the first to report that the smallest Pt particles resulted in the highest uptake for spillover in MOF [52], further supported by L. Yang et al.'s work who found that small size Ni particles doped onto ACs were crucial for improving the hydrogen uptake [63], and by

Mukherjee et al. [64] who presented the most comprehensive study about size dependency and spillover. However apart from the size of the particles, other possible parameters such as the electronic state of the particle have not been investigated yet. Indeed, for platinum mainly, studies have shown that only the metal form was an active catalyst for hydrogenation [65]. Knowing the state of particles doped onto the adsorbent for hydrogen storage could then further give information about the possible occurrence of hydrogen dissociation, and then spillover.

1.4.2. Scope of this work and selection of materials

Metal organic framework-derived carbons are amorphous carbons with hierarchical pore structure. Because they present a high SSA with pore volume ranging from micropores to macropores and are lightweight, they represent promising candidate for hydrogen storage. Their intrinsically high sorption capacities compared to all other materials make them good candidates for testing a potential increase when doped with transition metal catalyst.

The choice of the metal catalyst is also of prime importance. As it is expected that both the MDC and the metal particle will have a role to play during the storage of hydrogen, it is important to choose one that does not form a stable hydride at ambient conditions.

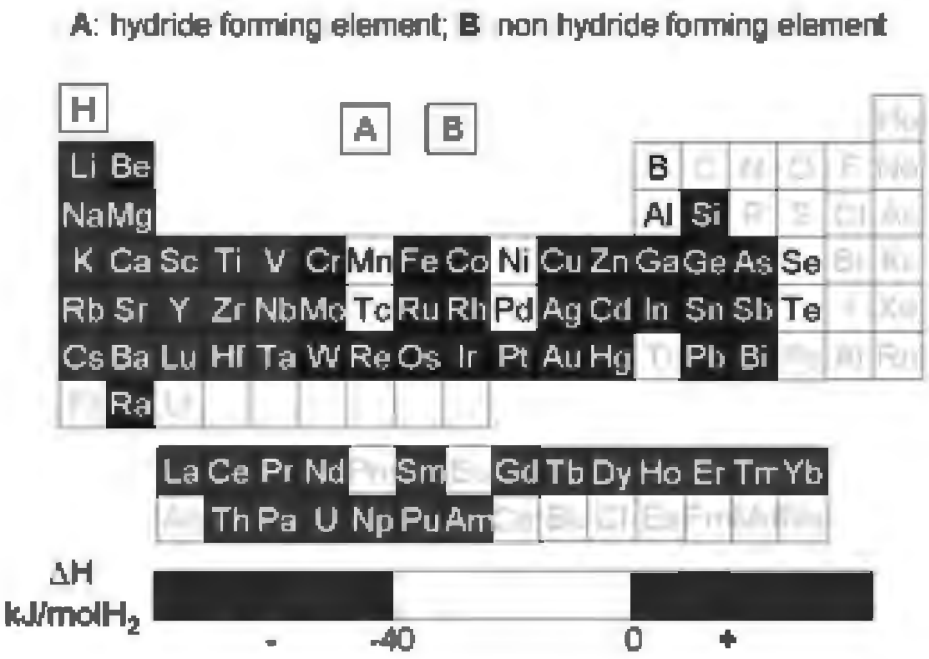

Figure 18: Hydride and non-hydride forming elements [6]

Figure 18 shows in dark blue the metals which would be of great interest. Moreover, platinum group metals are well known for their catalytic activities [66] and intervened in a plethora of studies for hydrogen dissociation. In a spillover point of view, platinum and palladium have proven their efficiency [62]. Platinum seems then to be the most appropriate transition metal to be hybridized with MDC.

MDCs are obtained by carbonizing MOFs at high temperature in order to lead to cubic shaped carbons with dimensions inferior to 500 µm. Due to their synthesis process and their shape, they could be hybridized with platinum in three main ways:

- The first one consists of coating Pt particles onto it or mixing with Pt particles, as for ACs or CNTs: this cannot really be called hybridizing then and the platinum particles cannot be dispersed onto and inside the MDC without making the structure collapse and without destroying its porosity.
- In the second one, the platinum precursor is mixed along with the MOF's one so that the final MDC product will contain Pt particles. This method would have been appealing if such high temperatures (900°C in case of MOF-5 in order to let the zinc building unit vaporize) were not used. Indeed, Pt particles growth and agglomeration occur typically at temperatures higher than the Tamman temperature, unless they are coated on some support where oxidized particles hold the platinum ones more securely and reduce migration and loss of SSA [41, 67, 68].
- A carbon support could also be used for platinum particles, and these Pt-doped on a support mixed with MOF's precursors in situ before the carbonization process.

The choice of that support is then crucial. First it has to be a carbon nanomaterial so that it does not affect the long range structure and texture of MDC and does not add additional dead mass (heavy material which would not participate to hydrogen storage) to the material. The

best candidates in that way are CNTs, graphene oxides (GO), activated carbons (ACs) and graphene or reduced graphene oxides. Then, it should allow for a uniform dispersion of Pt particles in the nanoscale (a uniform coating is more likely to give a uniform composite, and nanosized Pt particles are required for a good SSA). That uniform dispersion comes naturally with functional groups containing carbon materials that show a good dispersability in organic solvents which can contain the platinum precursor. Besides, these functionalities play a non-negligible role in Pt particles anchoring, hence minimizing their agglomeration and size growth during carbonization or long life utilization.

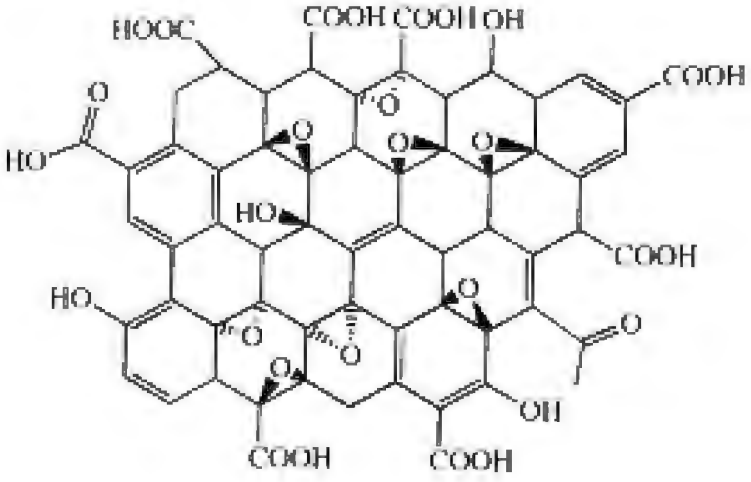

Figure 19: Graphene oxide

Among the supports previously cited, graphene oxide (GO) (Figure 19) is the most suitable one due to its unparalleled mass-producibility (from graphite oxide exfoliation), and its various kinds of oxygen functional

groups including hydroxyls, epoxies and carboxylic acid, which allow its exceptional dispersability in most of the polar solvents. Moreover, GO has been demonstrated to have a high affinity with the organic ligands of MOFs and hence can form stable composites with them [69]. Thermal treatment of GO is a route to obtain reduced graphene oxide whose structure approaches that of graphene. The material of our study will then be a composite material made of Pt particles-supported on reduced graphene oxide dispersed in the structure of MDC. Structural and textural characterization, electronic state analysis, thermo-gravimetric analysis (non-reported here), surface investigation and hydrogen sorption measurements will validate the synthesis of the composite material.

1.4.3. Expected value of this work

This work represents the first study of a MDC-based hybrid material investigated for hydrogen storage. Not only the feasibility and the performance of such system will be explored, but the electronic state of the Pt particles and their support will be revealed for the first time as well. Given the number of MDCs with hierarchical porosity and high SSA that can be synthesized from MOFs (hundreds), the results of this work could open a route to the investigation of the most promising of them and the role of their hybridization in hydrogen storage.

2. Experimental

2.1. Materials

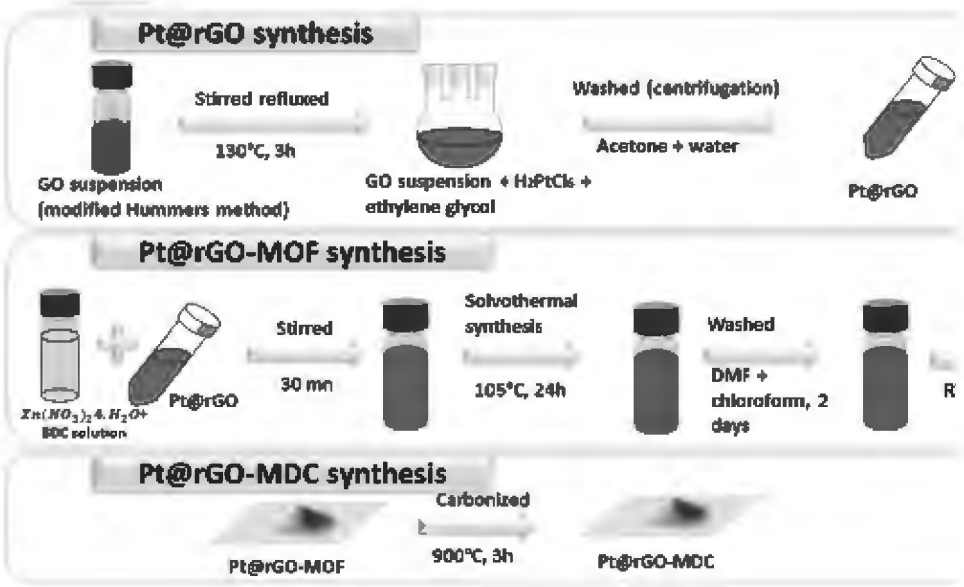

Figure 20: Experimental scheme

A scheme of the experimental protocol can be found in Figure 20.

2.1.1. Reagents and chemicals

1.1.1.1. For the synthesis of graphene oxide

The graphite precursor (flake, lot # MKBL8976V) was purchased from Sigma-Aldrid, and dried in a vacuum oven at 120°C for weeks before use. Potassium persulfate (98%), phosphorus pentoxide (98%) and potassium permanganate (98%) were purchased from Sigma-Aldrich, and stored in a desiccator before use. Concentrated sulfuric (98%),

hydrochloric acid (35%) and hydrogen peroxide solution (30%) was purchased from Daejung Chem. & Metal Co. Ltd. All chemicals were guaranteed grade for the analysis and used as received.

1.1.1.2. For the synthesis of metal-organic framework and metal-organic framework-derived carbon

The isoreticular MOF IRMOF-1, first element of the isoreticular family [70], was synthesized. The metal precursor zinc nitrate tetrahydrate was purchased from Sigma-Aldrich and stored in a glove box. The ligand precursor dicarboxylic acid (BDC) was purchased from Sigma-Aldrich and kept in a desiccator. Diethyl formamide, obtained from Tokyo Chemical Industry Co. Ltd., was used as a solvent and stored along with BDC. Anhydrous chloroform (95 %) purchased from Sigma-Aldrich and N,N-dimethylformamide from Daejung Chem. & Metal Co. Ltd were used to wash the synthesized IRMOF-1. All reagents were used as received without further purification.

2.1.2. For the synthesis of platinum-doped reduced graphene oxide

Chloroplatinic acid hydrate was used as the metal precursor; ethylene glycol as the reducing agent, diethyl formamide as the solvent, and 4,4'biipyridine as an agent allowing better anchoring of the as reduced platinum particles. All these reagents were purchased from Sigma

Aldric and stored in a desiccator for further use. Sodium hydroxide, purchased from ---, was used to maintain the pH of the solution basic.

2.1.3. Synthesis of graphene oxide (GO)

GO was synthesized from graphite by a modified Hummer's method. Graphite was first pre-oxidized. 2 g of graphite flake being added slowly into sulfuric acid (20 ml) where $K_2S_2O_8$ (4 g) and P_2O_5 (4 g) were completely dissolved. The mixture was kept at 80 °C for 72 h in an oil bath while stirring by 200-300 rpm. Next, the mixture was washed by deionized (DI) water (1 L) with vacuum filtration several times until neutralized and dried in vacuum oven at room temperature.

The obtained pre-oxidized graphite (2 g) was dispersed into concentrated sulfuric acid (92 ml) at 0 °C while stirring at 500 rpm and gradually adding 12 g of $KMnO_4$. After 2 h of stirring at 35 °C, the mixture was slowly diluted with DI water (200 ml) in order not to increase the temperature above 90 °C and stirred for 2 h. H_2O_2 (10 ml) was then slowly added to the mixture while keeping the temperature at 90 °C. The mixture was finally washed with HCl by centrifugation at 13000 rpm for 15 min. The procedure was repeated three times in order to eliminate Mn^+ ions and the final mixture was repeatedly washed five times with DI water to neutralize GO.

The product of this step is named GO (Figure 21).

2.1.4. Synthesis of Pt-doped reduced graphene oxide (Pt@rGO)

30 mg of GO dispersed in deionized water were transferred into DEF via solvent exchange using centrifugation. The centrifuge was set up for 13000 rpm during 20 min. After each turn the solvent color was eye-checked and re-centrifuged if not transparent. Once transparency occurred, the solvent was poured out and solvent exchange step repeated. The procedure was reiterated 3 times. The final solution contained 5 ml DEF.

4,4-dipyridine (60 mg) was added to the GO dispersion and the mixture was ultrasonically dispersed for 3 h. In the meantime, chloroplatinic acid hydrate (12.8 mg) and sodium hydroxide (450 mg) added to 25 ml ethylene glycol were stirred until obtaining a yellow-transparent mixture. That mixture was then added to a round-bottom flask along with the graphene oxide dispersion and stirred again for another 2 h before being stirred-refluxed at 130 °C for 2 h under nitrogen atmosphere.

The obtained dispersion of Pt-doped reduced graphene oxide is named Pt@rGO (Figure 21).

Pt@rGO was thoroughly washed in DEF before being dispersed in it (30 ml) via centrifugation and kept in a fridge for further use.Synthesis

of Pt-doped reduced graphene oxide in a metal organic framework (Pt@GO-MOF).

2.1.5. Synthesis of IRMOF-1 (MOF))

In a typical procedure of IRMOF-1 synthesis, zinc nitrate tetrahydrate (2.34 g) and dicarboxylic acid (0.51 g) were added to a vial containing 90 ml of DEF. The mixture was stirred until transparency and the vial was transferred to a furnace and heated at 105 °C for 24 h, at a heating rate of 2 °C/min, before being allowed to cool down at room temperature. The formed crystals were then successively washed with dimethylformamide (DMF) and chloroform. The final wash was followed by pore activation under nitrogen flow and the obtained crystals were then dried in a 120 °C vacuum oven for 24 h. The final product was stored in a room temperature vacuum oven for further use. In the following, IRMOF-1 will just be named MOF (Figure 21).

2.1.6. Synthesis of MDC-1 (MDC)

The synthesized MOF was carbonized at 900 °C for 3 h under nitrogen atmosphere. The heating rate was 5 °C/min. The furnace was let to cool down at room temperature and the obtained MDC-1 (labelled MDC in the following) powder was transferred to a room temperature vacuum oven and stored there for further use (Figure 21).

2.1.7. Synthesis of Pt- doped reduced graphene oxide in a metal organic framework (Pt@rGO-MOF)

10 ml of the Pt@rGO suspension was added to a vial of the transparent mixture of IRMOF-1 precursors (80 ml DEF, the amount of precursors being unchanged) and stirred for 30 min before being transferred to the furnace, all other following steps being the same as in a mere IRMOF-1 synthesis.

The product of this synthesis step is designated as Pt@rGO-MOF (Figure 21).

2.1.8. Synthesis of Pt- doped reduced graphene oxide in a metal organic framework-derived carbon (Pt@rGO-MDC)

The as synthesized Pt@rGO-MOF was carbonized following the same procedure as in the case of MDC-1, and resulted in a product which will be termed as Pt@rGO-MDC (Figure 21).

2.1.9. Synthesis of rGO-MOF and rGO-MDC

In order to separate the roles played by the reduced graphene oxide and the Pt catalysts in the storage of hydrogen, the uptake of GO-MDC was also investigated. Therefore, GO-MOF was synthesized following the same procedure as in Pt@rGO-MOF, but the 10ml suspension of Pt@rGO was replaced by a 10ml suspension of GO (10mg) in DEF.

The obtained rGO-MOF was carbonized to obtain rGO-MDC (Figure 21).

2.1.10. Synthesis of Pt-MOF and Pt-MDC

To further check the usefulness of the rGO support used for uniformity and particle growth minimization, a MDC-based hybrid material solely composed of the MDC and Pt particles, without the rGO support, was also synthesized.

Chloroplatinic acid (12.8 ml) added to a round bottom flask containing 20 ml of DEF was stirred and refluxed at 130°C under nitrogen flow for 3h. After the mixture cooled down, it was transferred to a vial and sodium borohydride (11 mg) was added under vigorous stirring. After 1 h, reduced Pt particles of diameter superior to 200 nm was filter using an anodisc filtering paper. The obtained solution was then added to a solution of 10 ml DEF containing BDC (17 mg) and zinc nitrate tetrahydrate (78 mg), and stirred for 30mn before being solvothermally treated following the same procedure as in MOF.

The synthesized Pt-MOF was carbonized following the same procedure as for MDC (Figure 21).

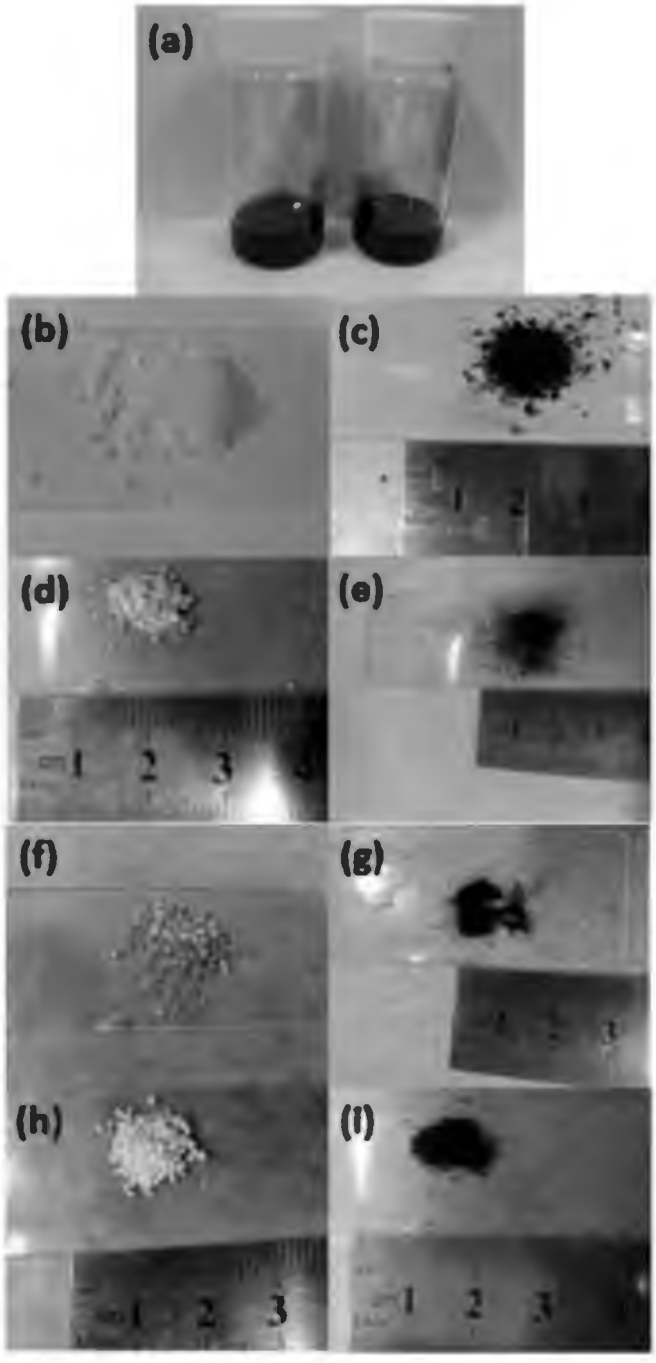

Figure 21:Samples synthesized all along the procedure to Pt@rGO-MDC: a)GO dispersion (left) and Pt@rGO dispersion (right), b)MOF, c)MDC, d)Pt@rGO-MOF, e)Pt@rGO-MDC, f)rGO-MOF, g)rGO-MDC, h)Pt-MOF, i)Pt-MDC

2.2. Analysis

2.2.1. Powder X-Ray diffraction (PXRD) pattern

PXRD profiles were obtained to (1) record a crystallographic change between the pristine materials and the hybrid ones and (2) give an approximation of the mean particle size of the Pt particles dispersed in the composites.

PXRD was carried out using a D8 Advance (Bruker) diffractometer. The diffractograms were recorded in a reflection mode using a Cu Kα radiation (λ=1.54184 Å) with a Ni filter.

2.2.2. Scanning Electron Microscopy (SEM) &

SEM and TEM measurements were performed to investigate the structural detail of the samples. The samples shape, size and structure were studied using a normal SEM equipment (JEOL-5600). The powdery samples were deposited on a carbon tape, which was itself stuck onto a SEM sample holder. Prior to the measurement, the non-platinum containing samples were decorated with platinum by sputtering.

2.2.3. Transmission Electron Microscopy (TEM)

The Pt particles size and distribution were obtained with an advanced Field Electron Microscope featuring (JEOL 2100 F). That dispositive provided also diffraction patterns and energy dispersive spectroscopy

(EDS) measurements which helped to detect the presence of platinum, amorphous carbon and graphene oxide mainly.

Prior to the measurements, the samples were sonicated into DMF (in a ratio 1:10) and dropwise (2 drops) added onto a copper grid holder, before being vacuum dried at 60°C for 24h at least.

2.2.4. X-Ray photoelectron Spectroscopy (XPS)

The XPS study was carried out to obtain the chemical composition of the sample and to quantify the functional groups and electronic state of the Pt particles.

The powdery samples were deposited onto a normal two-faced tape stuck onto a silicon wafer. These wafers were previously successively washed with acetone, isopropyl alcohol and deionized water by ultrasonication for 10 mn each and then died in a 60°C oven. To minimize the possible noises of the photoelectron signal, a toothpick was used to assure a uniform deposition.

The samples were further investigated with an AXIS-His, KRATOS spectrometer, and XPSPEAK41 software used for the peaks fitting and deconvolution.

2.2.5. Nitrogen adsorption (BET SSA)

Nitrogen adsorption data were obtained to evaluate the apparent surface area based both on the BET and the Langmuir equations, and the porosity.

Nitrogen adsorption isotherms at 77 K up to 1 bar were measured using a Micromeritics ASAP 2020 static volumetric gas adsorption instrument. The pore size distribution of the samples were assessed using non-local density functional theory (NLDFT) as described in [35]. All sorption isotherms were obtained using ultrahigh purity nitrogen gas (99.999 %). Prior to the sorption analysis, samples in the analysis chamber were vacuum-dried at 150 °C under a pressure of 10–5 Torr for 12 h.

2.2.6. Hydrogen sorption (Rubotherm Gravimetric apparatus)

Due to the huge errors inherent to a volumetric system [71-74], gravimetric measurements were performed at room temperature and pressures up to 100 bar, using a magnetically suspended microbalance (Rubotherm, Bochum, Germany) [75].

Prior to the gravimetric analyses, the samples were degased under vacuum at 150 °C for 12h. The pressure was then increased step by step up to 30 bar (0 – 5 – 10 – 30 bar), under Helium gas in order to measure the buoyancy effect and then decreased again to vacuum (30 –

1 – 0 bar). After buoyancy measurement, Hydrogen was loader by increasing the pressure step by step (0 -1 – 5 – 10 – 30 – 50 – 70 – 100 bar) before decreasing it (100 – 50 – 1 – 0 bar). At each step, the applied pressure was hold for 30 min to 1h in order to allow complete saturation.

All sorption isotherms were obtained using ultrahigh purity gases (99.999 %).

3. Results and Discussion

3.1. Morphology

The first step of synthesizing the MDC based hybrid material corresponds to the loading of Pt particles onto the graphene oxide support. The Pt@rGO dispersion looks darker than the primary GO dispersion (which is brown) (Figure 21). A darker solution typically means a reduction in the number of functional groups implying that GO has been _at least partially_ reduced to form reduced graphene oxide. This motivated the choice of naming the Pt particles loaded onto the GO flakes Pt@rGO instead of Pt@GO. Despite the reduction of number of functional groups, Pt@rGO showed a good dispersability in DEF solvent (Figure 21).

The ideal final hybrid material to be obtained must be a cubic shaped amorphous carbon in which Pt-loaded rGO flakes are dispersed. The synthesis of such material can be eye-checked from the intermediary compounds. Indeed, as can be seen in Figure 21 which shows the final products obtained at each step, MOFs are white-yellow cubic-shaped crystals, slightly transparent. The crystals obtained from the same vial display the same average size. When their structure accommodates Pt-loaded rGO flakes or rGO flakes, their color turns to grey and their shape remains cubic with however a less uniform size distribution, and

the smaller the crystal, the darker it turns. The focus on a single framework through SEM investigation (Figure 23) confirms the retainment of the cubic shape.

The grey color suggests that the MOFs' framework built itself around the Pt-loaded rGO sheets in the solution, these might have served as seeds for crystallization. The long range synthesis do not seem to be affected as the cubic shaped was retained, but the variation in crystal size of the composite materials as well as their apparent non-uniformity in the case of Pt@rGO-MOF might be due to the concentration of Pt@rGO or rGO sheets in the MOFs' precursors solution. Indeed, as the distribution of rGO sheets is more uniform than that of Pt@rGO ones (because of a higher number of functional groups), the concentration of MOFs' precursors in the solution is also more uniform. Let MOFs crystals form around an average number of rGO flakes in the solution, the available MOF's precursors remain slightly the same in the whole solution, letting basically the same room for each rGO-MOF framework building (Figure 22). In the case of Pt@rGO-MOF, here too let MOFs crystals form around the same average number of Pt@rGO flakes in the solution, these ones showing a slightly inferior dispersability, the available MOFs precursors in the solution is higher at some places, letting the formed framework to be slightly bigger (Figure 22).

Figure 22: Schematic representation of rGO-MOF (left) and Pt@rGO-MOF (right) synthesis solutions

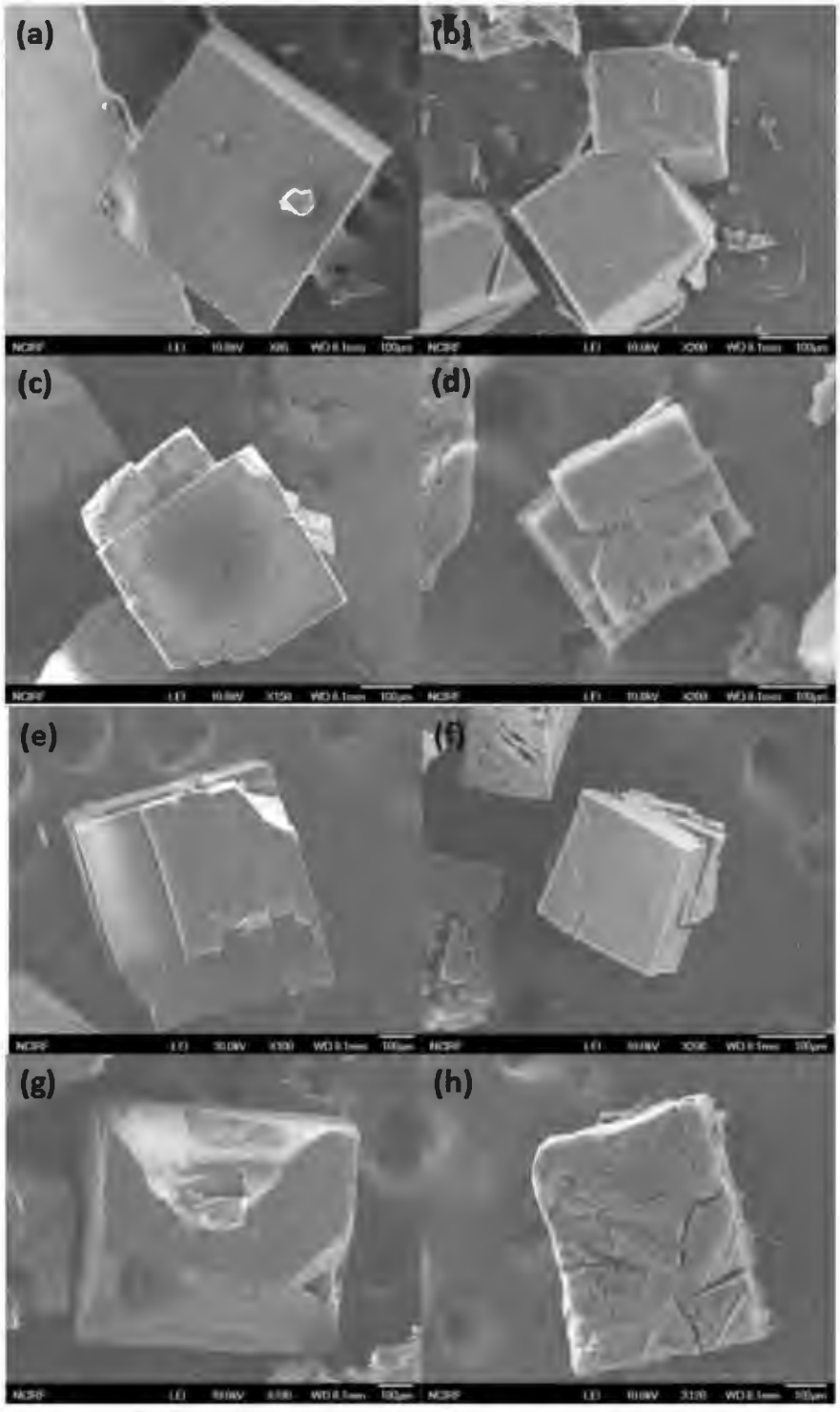

Figure 23: SEM micrographs with global view of synthesized framework: a)MOF, b)MDC, c)Pt@rGO-MOF, d)Pt@rGO-MDC, e)rGO-MOF, f)rGO-MDC, g)Pt-MOF, h)Pt-MDC

As the cubic shape of MOFs remains after carbonization for MDCs synthesis [76], it shall also remain during the carbonization of Pt@rGO-MDC and rGO-MDC. Figure 23 shows the silhouette of the samples, with a cubic shape for all of them and a change in the framework size as noticed above.

3.2. Structure

A composition analysis obtained from XPS measurements revealed that 8.3 wt. % Pt was loaded onto rGO flakes. As can be seen in Figure 24, the graphene oxide peak at $2\theta = 10.4°$ does not appear in the Pt@rGO sample suggesting that the graphene oxide was reduced. A low intensity peak appears at $2\theta = 39.6°$, characteristic of Pt (111) crystallographic plane. The almost invisible peak is probably due to finely dispersed nano-sized Pt particles.

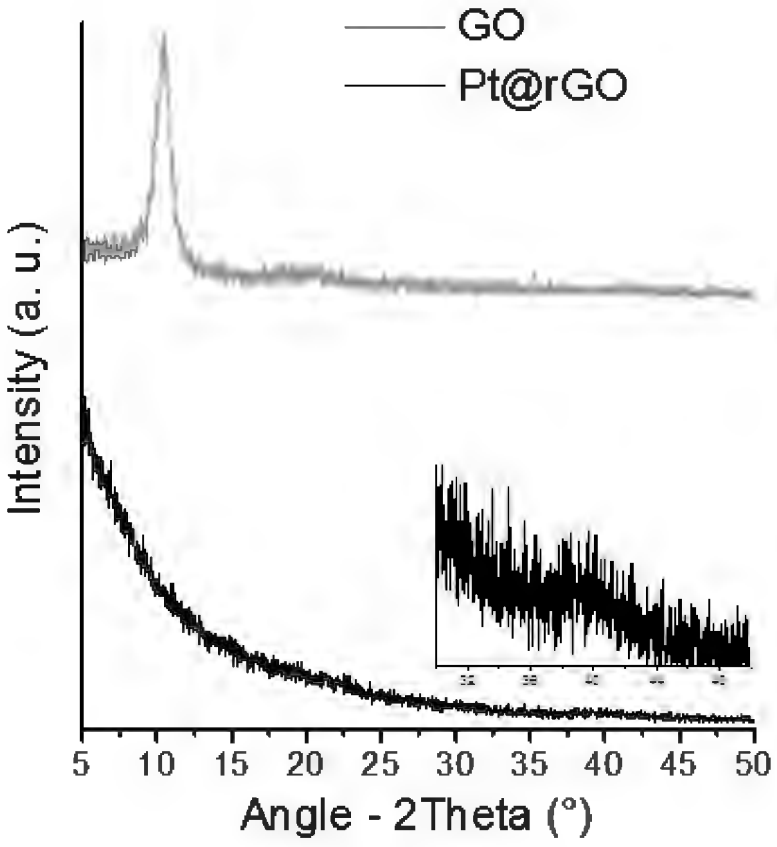

Figure 24: XRD pattern of GO and Pt@rGO

A PXRD analysis of both MOF and Pt@rGO-MOF (Figure 25) shows that the main peaks of MOF were maintained through the composite synthesis, with however a change in the intensity indicating a less oriented structured. Some preferred orientations became less present at the expense of other primarily less present in the pristine MOF material. The recovery of almost all peaks however implied that the long range structure was conserved. Here too, Pt particles are barely detected but appear clearly in the zoomed area (Figure 25). The very low intensity could also be due to the low concentration of platinum in MOF.

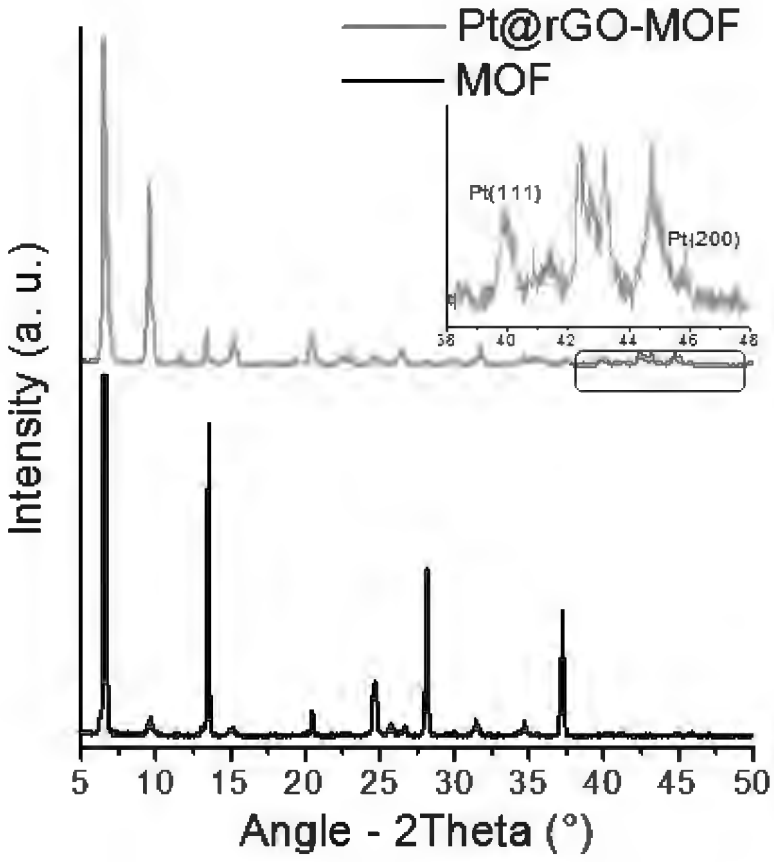

Figure 25: XRD pattern of MOF & Pt@rGO-MOF

The XRD pattern of MDC and Pt@rGO-MDC can be found in Figure 26. The amorphous MDC diffraction pattern is retained in Pt@rGO-MDC as expected. A broad and barely visible XRD peak ranging from 2θ = 38 ° to 2θ = 48 ° in the Pt@rGO-MDC diffraction pattern suggests a merging of the peaks of Pt(111) at and Pt(200) planes at 2θ =39.7 ° and 46.2° respectively. Its width and low intensity could be due to finely dispersed nano-sized Pt particles too, just like in Pt@rGO sample.

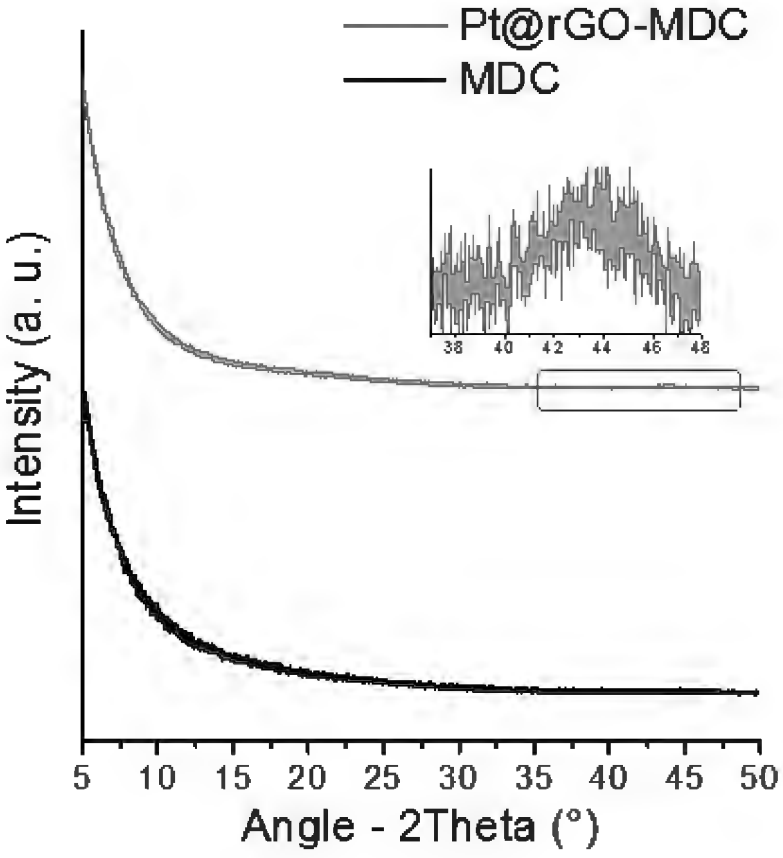

Figure 26: XRD pattern of MDC and Pt@rGO-MDC

3.3. Platinum particles doping and role of the substrate

TEM images give a better insight in the Pt particles' size and distribution. As can be seen in Figure 27, Pt particles are very well dispersed in both Pt@rGO and Pt@rGO-MDC samples, with an average particle size taking values from 1 to 3 nm. No significant

particle growth seems to have occurred, even after the heat treatment up to 900°C.

The minimization of the growth of particles size could mainly mean that those particles are well anchored onto the rGO surface on which the functionalities primarily present bind enough strongly the Pt particles. This assumption is further checked by synthesizing a composite material solely composed with Pt particles and MDC, in situ, by first going through the synthesis of a Pt-MOF hybrid material which will be carbonized. The TEM images of these Pt-MOF and Pt-MDC materials are displayed in Figure 28. The Pt-MOF one, which did not undertake the harsh thermal treatment up to 900°C, has a quite uniform Pt particles distribution with an average diameter size of ~5nm, while Pt-MDC shows a highly non-uniform Pt dispersion with particles size ranging from around 5 to 25 nm.

The reduced graphene oxide support was then efficient in synthesizing a MDC-based hybrid material with uniform distribution of nano-sized Pt particles, which did not suffer very much from the thermal treatment.

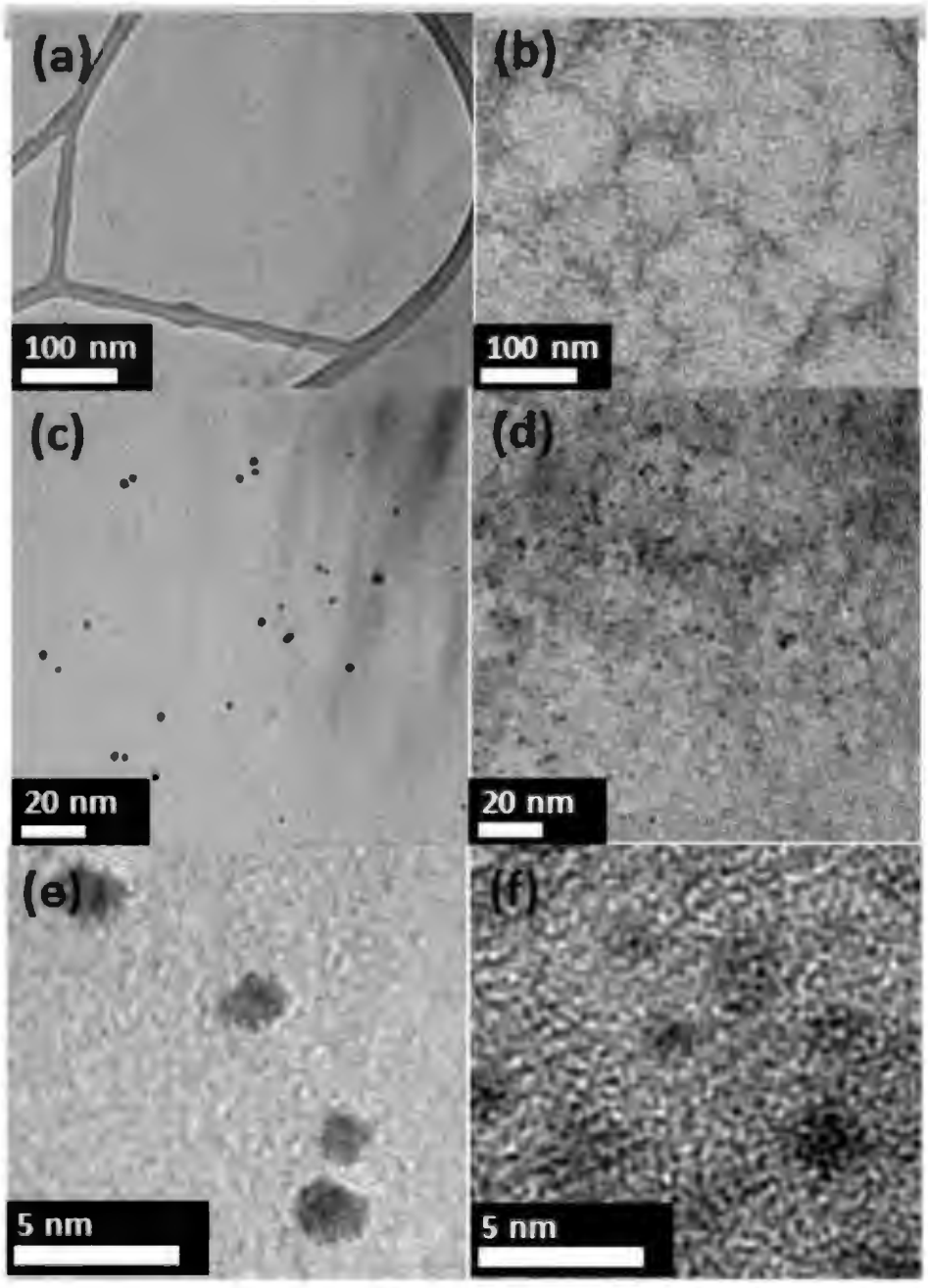

Figure 27: TEM images of Pt@rGO (a,c,e) and Pt@rGO-MDC (b,d,f) under different magnifications

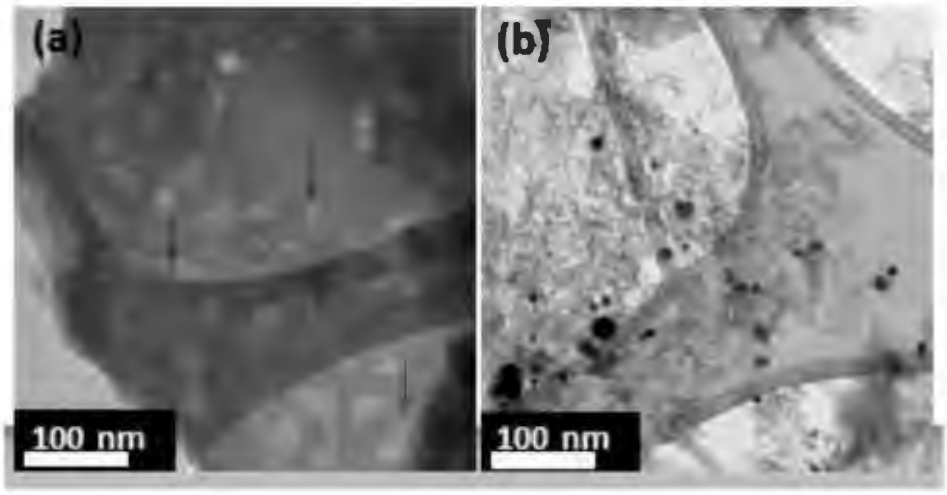

Figure 28: TEM images of Pt-MOF (left) and Pt-MDC (right)

3.4. Electronic state, chemical state and functionalities characterization

The well dispersed Pt particles and their rGO support were investigated with X-Ray photospectroscopy. Apart from informing about the chemical composition of each sample (8.3 wt. % Pt were loaded onto rGO and 4.3 wt. % Pt were present in Pt@rGO-MDC), the XPS analysis further lightens the binding relationship between the metal particles and their support. Platinum metal, and not platinum oxides, acts as the active catalytic site [65] during hydrogenation. The composite Pt@rGO-MDC which is to be synthesized should then have the highest quantity of platinum metal (Pt(0)) possible, meaning only some portion of the loaded platinum should be allowed to be in an oxidized state.

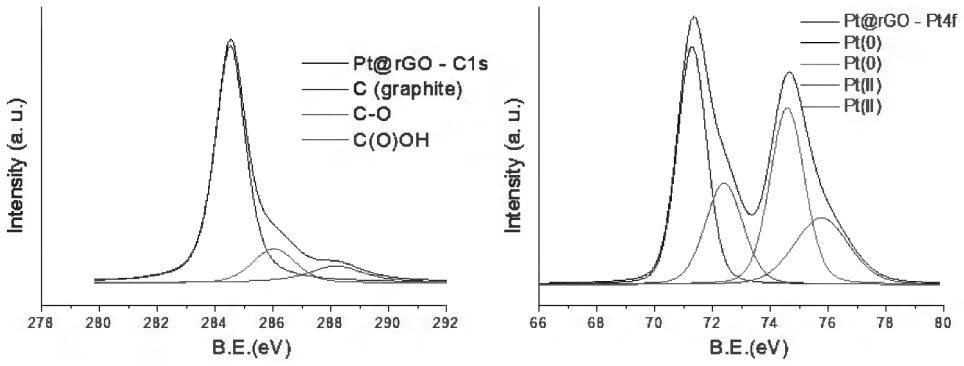

Figure 29: XPS spectra of Pt@rGO: C1s (left) and Pt4f (right)

Figure 29 shows the C1s peak of Pt@rGO and its deconvolution. As stated previously, the number of functional groups at the surface of the primary graphene oxide (Figure 29) decreased, meaning that GO was reduced during the metal loading process. This reduction could have two causes. One is the temperature used for coating Pt onto GO (130 °C) combined with the loading time (2 h). Typically such low temperature does not usually reduce GO totally (as in Figure 29) unless the heating duration lasted a while, even if it highly depends on the nature of the GO used. The second one is a redox reaction that might have occurred between GO (or rather its functional groups) and non-reduced platinum ions in the solution.

Table 3: Oxidation state of carbon and platinum on different samples

Samples	Quantity Pt(0), %	Quantity Pt(II), %
Pt@rGO	64	36
Pt@rGO-MDC	83	17

Figure 30 suggests that both processes took place: the thermal reduction as well as the redox reaction. Indeed, a GO sample was tested to undertake the same thermal treatment without Pt loading (2 h thermal treatment at 130 °C), see Figure 30.The Th-rGO that resulted from that thermal treatment was not totally reduced and still had a non-negligible amount of functional groups. The heat treatment was then only partially responsible for the reduction of GO.

When looking through the deconvoluted Pt4f peak in the Pt@rGO sample, it can be noticed that a high amount of Pt was still oxidized (36 %), despite the predominance of ethylene glycol reducing agent in the solution (443 mmol for 25 µmol of Pt). This supports the assumption that reduced platinum particles reacted with oxide functionalities at the surface of GO, suggesting that in addition to the thermal treatment, a redox reaction between reduced platinum particles and GO functionalities leaded to the previously noticed reduction of

GO during the loading process. That redox reaction helped better anchoring of platinum onto rGO, possibly minimizing their agglomeration and at the same time the surface energy barrier for a possible migration of hydrogen from the metal particles to the support.

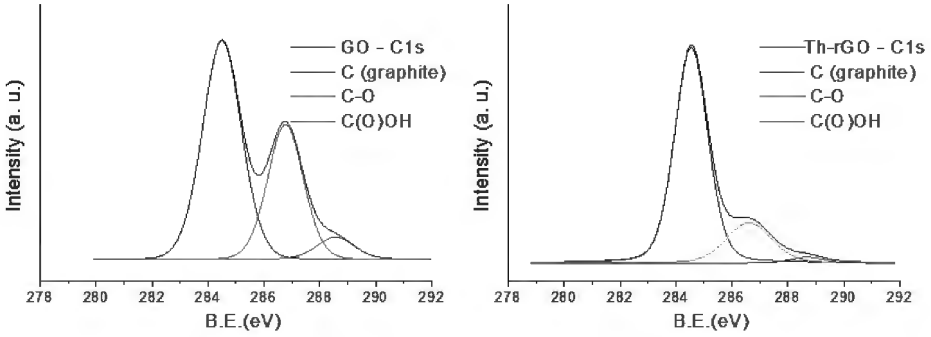

Figure 30: C1s XPS spectra of GO (left) and thermally treated GO (right)

When Pt@rGO is incorporated into MOF and the sample undertakes a new thermal treatment to give Pt@rGO-MDC, the Pt particles are further reduced as can be seen in Figure 31. A higher portion of the incorporated Pt particles in Pt@rGO-MDC material are then in their metal form (Table 3), that is their active catalyst form.

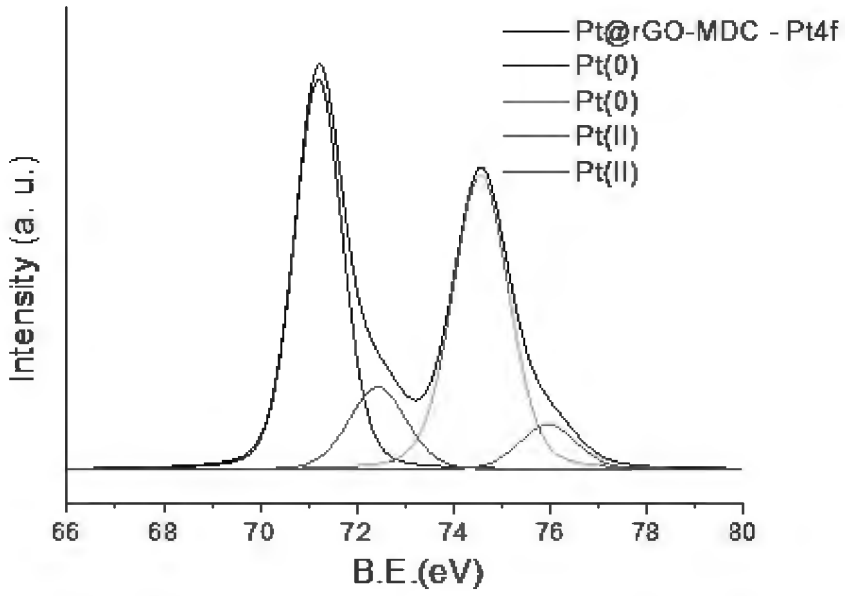

Figure 31: Pt4f XPS spectrum of Pt@rGO-MDC

3.5. Textural characteristics

Nitrogen adsorption isotherms, at 77 K, of MDC, Pt-MDC, Pt@rGO-MDC and rGO-MDC are shown in Figure 32. All the samples exhibited a type IV isotherm. The low pressure region indicates the presence of macro- and mesoporosity in which multilayer adsorption of N_2 can take place. The high pressure region indicates the presence of microporosity in which adsorption takes place by capillary condensation. This proves the hierarchically porous structure of MDC [35] and shows that that hierarchical porosity is maintained in Pt@rGO-MDC and Pt-MDC. The barely noticeable inflexion point in the isotherm of Pt-MDC at higher pressures indicates that the number of micropores, in which capillary

condensation favors a multilayer adsorption, decreases; and the well-defined plateau in the isotherm of Pt@rGO at higher pressures indicates a higher multilayer adsorption and subsequently a higher volume of micropores.

These assumptions are further checked by calculating the BET surface area as well as the pores volume. Pt@rGO-MDC exhibited the same micropores volume as MDC, indicating that the incorporation of Pt@rGO flakes only affects the macro- and mesoporosity. Indeed, as Pt@rGO flakes are believed to serve as nucleation sites for the formation of MOF as stated previously, their incorporation induces the formation of mesoporosity due to their size. rGO-MDC exhibits the highest micropores volume, hence the more defined type IV isotherm. Pt-MDC, for its part, suffers a decrease in all its range of porosity. This can be due to Pt particles obstructing its porosity. The higher surface area in rGO-MDC and in Pt@rGO-MDC compared to MDC and Pt-MDC can also be due to the presence of rGO, whose SSA contributes to the texture of the final composites obtained.

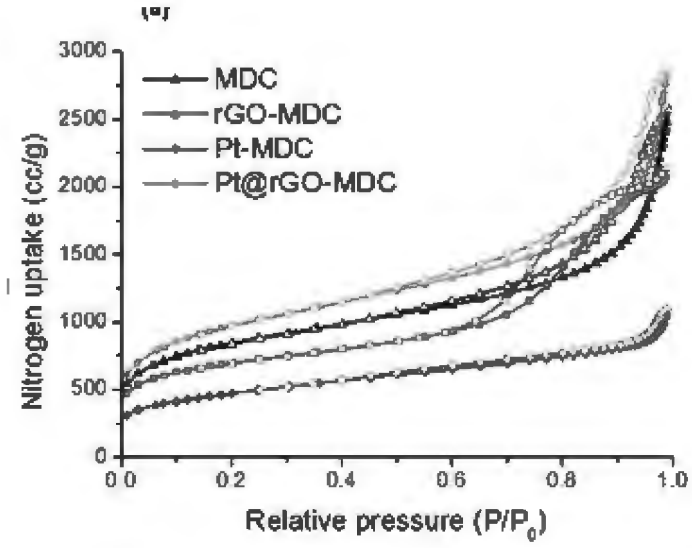

Figure 32: Nitrogen adsorption isotherms of MDC, Pt@rGO-MDC andPt-MDC

Table 4: Textural characteristics of MDC, Pt@rGO-MDC and Pt-MDC

Material	**Porosity cm^3/g**	**Microporosity cm^3/g**	**BET SSA m^2/g**
MDC	3.97	0.38	3006
Pt-MDC	1.69	0.16	1675
rGO-MDC	3.24	0.42	2452
Pt-rGO-MDC	4.42	0.37	3478

3.6. Hydrogen sorption properties

All hydrogen isotherms were taken at room temperature, typically at 28 °C, and pressures up to 100 bar (Figure 33), this in order to be as close as possible to the required conditions for on-board applications. The MDC synthesized stores 0.87 wt. % H_2 at these conditions. This value is also comparable to that reported previously, 0.94 wt. % H_2 [34].

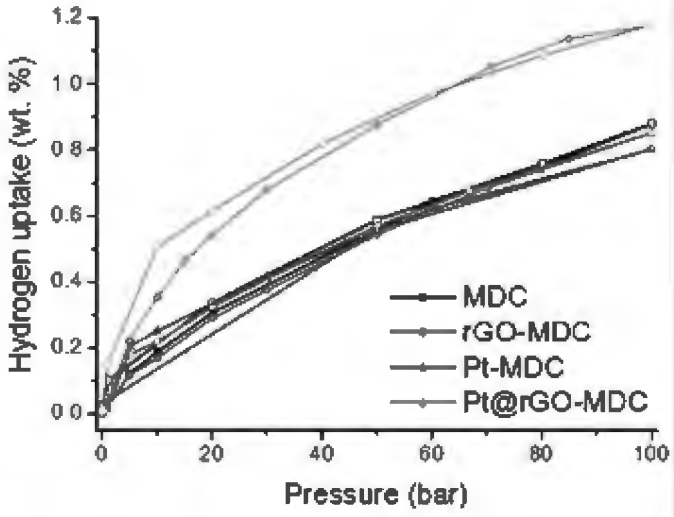

Figure 33: Hydrogen sorption isotherms of MDC, Pt@rGO-MDC and Pt-MDC

Based only on textural characteristics, the synthesized MDC should store more hydrogen than its mates. It however stores almost the same amount of hydrogen. The incorporation of rGO in the framework of MDC does not seem to benefit the storage capacity of MDC. Pt-MDC however, even with the really low surface area and pores volume,

shows the same storage capacity, meaning that the decrease in surface area was compensated with the loading of Pt particles.

Pt@rGO-MDC, in turn, stores up to 1.17 wt. % H_2 at RT and 100 bar, which represents an enhancement of 34 % compared to pristine MDC. The overall hydrogen uptake was then increased by doping the amorphous carbon MDC with Pt particles, and further by assuring a uniform dispersion of these particles at the nanoscale. The increase was significant (around 1/3), leading to a storage capacity greater than 1 wt. % at room temperature.

To prove the reversibility of the isotherms, the pressure was decreased back to 0 bar after having reached 100 bar. The isotherms in Figure 33 are totally reversible. In the experimental procedure, the pressure is increased step by step until the final pressure of 100 bar before being decreased back to 0 bar. At 0 bar, no more hydrogen remained in the samples, proving the total reversibility of the uptake. When looking more through the uptake, a slight hysteresis seems to take place. This is more due to the abrupt decrease of pressure _backwards, the steps did not follow 100 – 70 – 50 – 30 – 10 – 5 – 1 – 0 bar as in forwards case_ rather than the behavior of the material itself.

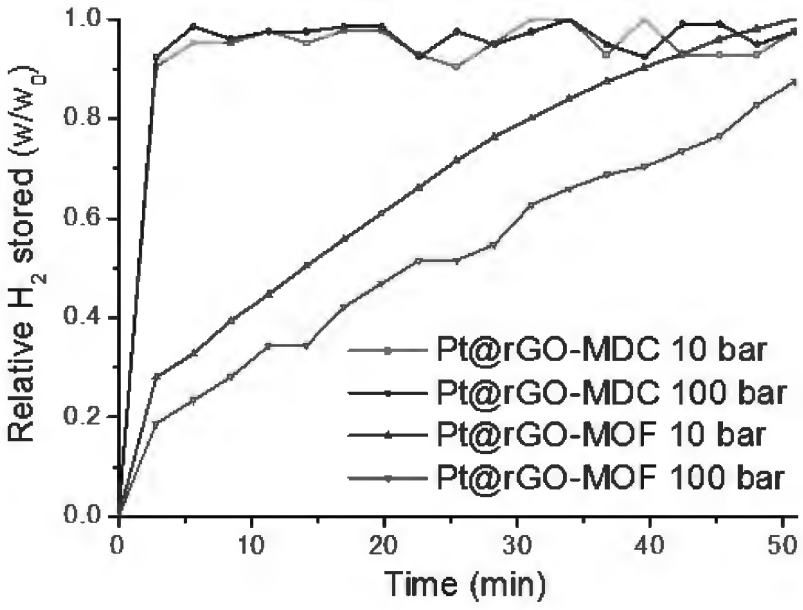

Figure 34: Kinetics of hydrogen adsorption in MDC, Pt@rGO-MDC, Pt-MDC

Figure 34 shows the kinetics of the adsorption. Pt-doped carbon materials used for hydrogen storage are known for having very slow kinetics, as it takes few hours to reach saturation [40]. That was not the case of Pt@rGO-MDC, which showed the same kinetics as MDC (Figure 34) at both low and high pressure (10 bar and 100 bar). Equilibrium was reached within 2.9 minutes. The fast kinetics of Pt@rGO-MDC were compared with that of the synthesized Pt@rGO-MOF, which acted as a reference as many reports on the spillover in Pt doped onto a carbon support and included in MOFs exist in the literature. While it took less than 3 minutes for Pt@rGO-MDC and MDC to reach saturation, Pt@rGO-MOF reached saturation after an

hour. The carbonaceous nature of both MDC and rGO was then relevant in minimizing surface energy barrier, compared to rGO and MOF.

Apart from an increased hydrogen uptake, reversibility and fast kinetics constitute key findings because these two factors together, sine qua non conditions for on-board applications, were barely reported in previous works dealing with transition metal doping on carbonaceous materials for hydrogen storage.

Pt particles definitely played a role in the uptake of hydrogen, which was to enhance to capacity of hydrogen storage.

4. Conclusion

This work dealt with recent concerns on finding a viable hydrogen storage system for on-board applications. It has been discussed than among all the up-to-now available systems _compressed gaseous hydrogen, liquid hydrogen, hydride systems and carbonaceous physisorptive systems_ the latter ones seem highly promising due to their safety, their mass-production capacity, their light weight, their reversible hydrogen uptake and their fast sorption kinetics. The only dark spot that hinders their use concerns their very low uptake capacity at room temperature (< 1 wt. % H_2 compared to the 5.5 wt. % targeted). Strategies to enhance this low uptake regroup the transition metals doping _ platinum for most of the cases_ which has proven its efficiency. This strategy faces however a certain number of limitations:

- The non-consistency of the results mainly due to the lack of understanding of the mechanism that allows such enhancement.
- The lack of study on the incorporated platinum state, regarding the fact that only platinum metal is an active catalyst.
- The numerous studies on carbon nanomaterials such as CNTs or ACs which, even after enhancement, show a lower capacity than MDC
- The lack of study on MDC

- Sluggish kinetics and/or non-reversibility

All these raisons motivated us to synthesize the first MDC-derived hybrid material (namely Pt@rGO-MDC) with well dispersed Pt particles via an anchoring onto rGO sheets.

The as synthesized material was thoroughly investigated and showed acceptable morphology, structure and texture for hydrogen storage. Pt@rGO-MDC exhibited a storage capacity of 1.17 wt. % H_2 at room temperature and 100 bar, representing an enhancement of 34% compared to the pristine MDC. Moreover, the hydrogen adsorption was totally reversible and the saturation was reached within 3 minutes, proving really fast kinetics.

One should keep in mind that the showed results were not meant to be optimized. This is evidenced by the smaller uptake of the pristine MDC compared to the literature. Besides, the 1.17 wt. % H_2 stored in Pt@rGO-MDC are still far from the gravimetric targets set by the U.S. DOE, but these above results showed for the first time that MDC can be successfully hybridized and the resulting hybrid material shows enhanced uptake, while keeping all the advantages of the pristine MDC (cheap, light, fast kinetics and total reversibility).

References

1. Dutta, S., *A review on production, storage of hydrogen and its utilization as an energy resource.* Journal of Industrial and Engineering Chemistry, 2014. **20**(4): p. 1148-1156.
2. Ni, M., et al., *Potential of renewable hydrogen production for energy supply in Hong Kong.* International Journal of Hydrogen Energy, 2006. **31**(10): p. 1401-1412.
3. Graetz, J., *New approaches to hydrogen storage.* Chemical Society Reviews, 2009. **38**(1): p. 73-82.
4. Langmi, H.W., et al., *Hydrogen Storage in Metal-Organic Frameworks: A Review.* Electrochimica Acta, 2014. **128**(0): p. 368-392.
5. Eberle, U., M. Felderhoff, and F. Schuth, *Chemical and physical solutions for hydrogen storage.* Angew Chem Int Ed Engl, 2009. **48**(36): p. 6608-30.
6. Dornheim, M., *Thermodynamics of Metal Hydrides: Tailoring Reaction Enthalpies of Hydrogen Storage Materials*. Thermodynamics - Interaction Studies - Solids, Liquids and Gases. 2011.

7. Lazicki, A., et al., *Static compression of LiH to 250 GPa.* Physical Review B, 2012. **85**(5): p. 054103.

8. Song, Y., *New perspectives on potential hydrogen storage materials using high pressure.* Physical Chemistry Chemical Physics, 2013. **15**(35): p. 14524-14547.

9. Fátay, D., Á. Révész, and T. Spassov, *Particle size and catalytic effect on the dehydriding of MgH2.* Journal of Alloys and Compounds, 2005. **399**(1–2): p. 237-241.

10. Baldi, A. and B. Dam, *Thin film metal hydrides for hydrogen storage applications.* Journal of Materials Chemistry, 2011. **21**(12): p. 4021-4026.

11. Srinivasan, S.S., et al., *Long term cycling behavior of titanium doped NaAlH4 prepared through solvent mediated milling of NaH and Al with titanium dopant precursors.* Journal of Alloys and Compounds, 2004. **377**(1–2): p. 283-289.

12. Orimo, S.-i., et al., *Complex Hydrides for Hydrogen Storage.* Chemical Reviews, 2007. **107**(10): p. 4111-4132.

13. Chen, P., et al., *Interaction of hydrogen with metal nitrides and imides.* Nature, 2002. **420**(6913): p. 302-304.

14. Yang, B., Y.-P. He, and Y.-P. Zhao, *Hydrogenation of magnesium nanoblades: The effect of concentration dependent hydrogen diffusion.* Applied Physics Letters, 2011. **98**(8): p. -.

15. Jorge Jr, A.M., et al., *An investigation of hydrogen storage in a magnesium-based alloy processed by equal-channel angular pressing.* International Journal of Hydrogen Energy, 2013. **38**(20): p. 8306-8312.

16. Liu, T., et al., *Synthesis and hydrogen storage properties of Mg–10.6La–3.5Ni nanoparticles.* Journal of Power Sources, 2014. **246**(0): p. 277-282.

17. Graetz, J., et al., *Kinetics and thermodynamics of the aluminum hydride polymorphs.* Journal of Alloys and Compounds, 2007. **446–447**(0): p. 271-275.

18. Graetz, J., et al., *Aluminum hydride as a hydrogen and energy storage material: Past, present and future.* Journal of Alloys and Compounds, 2011. **509, Supplement 2**(0): p. S517-S528.

19. Makowski, P., et al., *Organic materials for hydrogen storage applications: from physisorption on organic solids to chemisorption in organic molecules.* Energy & Environmental Science, 2009. **2**(5): p. 480-490.

20. Yang, S.J., et al., *Recent advances in hydrogen storage technologies based on nanoporous carbon materials.* Progress in Natural Science: Materials International, 2012. **22**(6): p. 631-638.

21. Dillon, A.C., et al., *Storage of hydrogen in single-walled carbon nanotubes.* Nature, 1997. **386**(6623): p. 377-379.

22. Chambers, A., et al., *Hydrogen Storage in Graphite Nanofibers.* The Journal of Physical Chemistry B, 1998. **102**(22): p. 4253-4256.

23. Liu, C., et al., *Hydrogen storage in carbon nanotubes revisited.* Carbon, 2010. **48**(2): p. 452-455.

24. Jordá-Beneyto, M., et al., *Hydrogen storage on chemically activated carbons and carbon nanomaterials at high pressures.* Carbon, 2007. **45**(2): p. 293-303.

25. Nishihara, H., et al., *High-Pressure Hydrogen Storage in Zeolite-Templated Carbon.* The Journal of Physical Chemistry C, 2009. **113**(8): p. 3189-3196.

26. Farha, O.K., et al., *Metal–Organic Framework Materials with Ultrahigh Surface Areas: Is the Sky the Limit?* Journal of the American Chemical Society, 2012. **134**(36): p. 15016-15021.

27. Rosi, N.L., et al., *Hydrogen Storage in Microporous Metal-Organic Frameworks.* Science, 2003. **300**(5622): p. 1127-1129.

28. Langmi, H.W., et al., *Hydrogen Storage in Metal-Organic Frameworks: A Review.* Electrochimica Acta, (0).

29. Dincă, M. and J.R. Long, *Hydrogen storage in microporous metal-organic frameworks with exposed metal sites.* Angewandte Chemie - International Edition, 2008. **47**(36): p. 6766-6779.

30. Zhao, D., D. Yuan, and H.-C. Zhou, *The current status of hydrogen storage in metal-organic frameworks.* Energy & Environmental Science, 2008. **1**(2): p. 222-235.

31. Murray, L.J., M. Dinca, and J.R. Long, *Hydrogen storage in metal-organic frameworks.* Chemical Society Reviews, 2009. **38**(5): p. 1294-1314.

32. Sculley, J., D. Yuan, and H.C. Zhou, *The current status of hydrogen storage in metal-organic frameworks - Updated.* Energy and Environmental Science, 2011. **4**(8): p. 2721-2735.

33. Suh, M.P., et al., *Hydrogen storage in metal-organic frameworks.* Chemical Reviews, 2012. **112**(2): p. 782-835.

34. Yang, S.J., et al., *General Relationship between Hydrogen Adsorption Capacities at 77 and 298 K and Pore Characteristics*

of the Porous Adsorbents. The Journal of Physical Chemistry C, 2012. **116**(19): p. 10529-10540.

35. Yang, S.J., et al., *MOF-Derived Hierarchically Porous Carbon with Exceptional Porosity and Hydrogen Storage Capacity.* Chemistry of Materials, 2012. **24**(3): p. 464-470.

36. Bhatia, S.K. and A.L. Myers, *Optimum conditions for adsorptive storage.* Langmuir, 2006. **22**(4): p. 1688-700.

37. Lueking, A. and R.T. Yang, *Hydrogen Spillover from a Metal Oxide Catalyst onto Carbon Nanotubes—Implications for Hydrogen Storage.* Journal of Catalysis, 2002. **206**(1): p. 165-168.

38. Khoobiar, S., *Particle to Particle Migration of Hydrogen Atoms on Platinum—Alumina Catalysts from Particle to Neighboring Particles.* The Journal of Physical Chemistry, 1964. **68**(2): p. 411-412.

39. Sermon, P.A. and G.C. Bond, *Hydrogen Spillover.* Catalysis Reviews, 1974. **8**(1): p. 211-239.

40. Srinivas, S.T. and P.K. Rao, *Direct Observation of Hydrogen Spillover on Carbon-Supported Platinum and Its Influence on the Hydrogenation of Benzene.* Journal of Catalysis, 1994. **148**(2): p. 470-477.

41. Torres, G.C., et al., *Effect of the carbon pre-treatment on the properties and performance for nitrobenzene hydrogenation of Pt/C catalysts.* Applied Catalysis A: General, 1997. **161**(1–2): p. 213-226.

42. Schwarz, J.A., *Metal assisted carbon cold storage of hydrogen.* 1988, Google Patents.

43. Yang, F.H. and R.T. Yang, *Ab initio molecular orbital study of adsorption of atomic hydrogen on graphite:: Insight into hydrogen storage in carbon nanotubes.* Carbon, 2002. **40**(3): p. 437-444.

44. Conner, W.C. and J.L. Falconer, *Spillover in Heterogeneous Catalysis.* Chemical Reviews, 1995. **95**(3): p. 759-788.

45. Wang, L. and R.T. Yang, *Hydrogen Storage on Carbon-Based Adsorbents and Storage at Ambient Temperature by Hydrogen Spillover.* Catalysis Reviews, 2010. **52**(4): p. 411-461.

46. Prins, R., *Hydrogen Spillover. Facts and Fiction.* Chemical Reviews, 2012. **112**(5): p. 2714-2738.

47. Lueking, A.D. and R.T. Yang, *Hydrogen spillover to enhance hydrogen storage—study of the effect of carbon physicochemical properties.* Applied Catalysis A: General, 2004. **265**(2): p. 259-268.

48. Li, Y. and R.T. Yang, *Significantly Enhanced Hydrogen Storage in Metal–Organic Frameworks via Spillover.* Journal of the American Chemical Society, 2005. **128**(3): p. 726-727.

49. Li, Y. and R.T. Yang, *Hydrogen Storage in Metal–Organic Frameworks by Bridged Hydrogen Spillover.* Journal of the American Chemical Society, 2006. **128**(25): p. 8136-8137.

50. Li, Y., F.H. Yang, and R.T. Yang, *Kinetics and Mechanistic Model for Hydrogen Spillover on Bridged Metal–Organic Frameworks.* The Journal of Physical Chemistry C, 2007. **111**(8): p. 3405-3411.

51. Li, Y., L. Wang, and R.T. Yang, *Response to "hydrogen adsorption in Pt catalyst/MOF-5 materials" by Luzan and Talyzin.* Microporous and Mesoporous Materials, 2010. **135**(1–3): p. 206-208.

52. Wang, L., et al., *Effects of Pt Particle Size on Hydrogen Storage on Pt-Doped Metal–Organic Framework IRMOF-8.* The Journal of Physical Chemistry C, 2011. **115**(11): p. 4793-4799.

53. Campesi, R., et al., *Hydrogen spillover measurements of unbridged and bridged metal-organic frameworks - Revisited.* Physical Chemistry Chemical Physics, 2010. **12**(35): p. 10457-10459.

54. Yang, S.J., et al., *Enhanced hydrogen storage capacity of Pt-loaded CNT@MOF-5 hybrid composites.* International Journal of Hydrogen Energy, 2010. **35**(23): p. 13062-13067.

55. Zhou, H., et al., *Enhanced room-temperature hydrogen storage capacity in Pt-loaded graphene oxide/HKUST-1 composites.* International Journal of Hydrogen Energy, 2014. **39**(5): p. 2160-2167.

56. Wang, L. and R.T. Yang, *New sorbents for hydrogen storage by hydrogen spillover - a review.* Energy & Environmental Science, 2008. **1**(2): p. 268-279.

57. Cheng, H., et al., *Hydrogen spillover in the context of hydrogen storage using solid-state materials.* Energy and Environmental Science, 2008. **1**(3): p. 338-354.

58. Contescu, C.I., et al., *Detection of Hydrogen Spillover in Palladium-Modified Activated Carbon Fibers during Hydrogen Adsorption.* The Journal of Physical Chemistry C, 2009. **113**(14): p. 5886-5890.

59. Tsao, C.-S., et al., *Neutron Scattering Methodology for Absolute Measurement of Room-Temperature Hydrogen Storage Capacity and Evidence for Spillover Effect in a Pt-Doped*

Activated Carbon. The Journal of Physical Chemistry Letters, 2010. **1**(10): p. 1569-1573.

60. Lee, H., et al., *In Situ Neutron Powder Diffraction and X-ray Photoelectron Spectroscopy Analyses on the Hydrogenation of MOF-5 by Pt-Doped Multiwalled Carbon Nanotubes.* The Journal of Physical Chemistry C, 2014. **118**(11): p. 5691-5699.

61. Tsao, C.S., et al., *Hydrogen spillover effect of pt-doped activated carbon studied by inelastic neutron scattering.* Journal of Physical Chemistry Letters, 2011. **2**(18): p. 2322-2325.

62. Psofogiannakis, G.M. and G.E. Froudakis, *Fundamental studies and perceptions on the spillover mechanism for hydrogen storage.* Chemical Communications, 2011. **47**(28): p. 7933-7943.

63. Yang, L., et al., *Effects of Ni Particle Size on Hydrogen Storage of Ni-Doped High Surface Area Activated Carbon.* Australian Journal of Chemistry, 2013. **66**(5): p. 548-554.

64. Mukherjee, S., B. Ramalingam, and S. Gangopadhyay, *Hydrogen spillover at sub-2 nm Pt nanoparticles by electrochemical hydrogen loading.* Journal of Materials Chemistry A, 2014. **2**(11): p. 3954-3960.

65. Scheeren, C.W., et al., *Hydrogen reduction of Adams' catalyst in ionic liquids: Formation and stabilization of Pt(0) nanoparticles.* Journal of Physical Chemistry C, 2008. **112**(42): p. 16463-16469.

66. Rao, C.R.K. and D.C. Trivedi, *Chemical and electrochemical depositions of platinum group metals and their applications.* Coordination Chemistry Reviews, 2005. **249**(5-6): p. 613-631.

67. Cameron, D.S., et al., *Carbons as supports for precious metal catalysts.* Catalysis Today, 1990. **7**(2): p. 113-137.

68. Antolini, E., *Formation, microstructural characteristics and stability of carbon supported platinum catalysts for low temperature fuel cells.* Journal of Materials Science, 2003. **38**(14): p. 2995-3005.

69. Petit, C. and T.J. Bandosz, *Exploring the coordination chemistry of MOF-graphite oxide composites and their applications as adsorbents.* Dalton Transactions, 2012. **41**(14): p. 4027-4035.

70. Li, H., et al., *Design and synthesis of an exceptionally stable and highly porous metal-organic framework.* Nature, 1999. **402**(6759): p. 276-279.

71. Weireld, G.D., M. Frère, and R. Jadot, *Automated determination of high-temperature and high-pressure gas*

adsorption isotherms using a magnetic suspension balance. Measurement Science and Technology, 1999. **10**(2): p. 117.

72. Belmabkhout, Y., M. Frère, and G.D. Weireld, *High-pressure adsorption measurements. A comparative study of the volumetric and gravimetric methods.* Measurement Science and Technology, 2004. **15**(5): p. 848.

73. Zlotea, C., P. Moretto, and T. Steriotis, *A Round Robin characterisation of the hydrogen sorption properties of a carbon based material.* International Journal of Hydrogen Energy, 2009. **34**(7): p. 3044-3057.

74. Demirocak, D.E., et al., *Volumetric hydrogen sorption measurements – Uncertainty error analysis and the importance of thermal equilibration time.* International Journal of Hydrogen Energy, 2013. **38**(3): p. 1469-1477.

75. Miller, M.A., C.-Y. Wang, and G.N. Merrill, *Experimental and Theoretical Investigation Into Hydrogen Storage via Spillover in IRMOF-8.* The Journal of Physical Chemistry C, 2009. **113**(8): p. 3222-3231.

76. Yang, S.J., et al., *Solvent evaporation mediated preparation of hierarchically porous metal organic framework-derived carbon*

with controllable and accessible large-scale porosity. Carbon, 2014. **71**(0): p. 294-302.